



Growth and erosion rates of the East Carpathians volcanoes constrained by numerical models: Tectonic and climatic implications

S. Dibacto, P. Lahitte, D. Karátson, M. Hencz, A. Szakács, T. Biró, I. Kovacs,
D. Veres

► To cite this version:

S. Dibacto, P. Lahitte, D. Karátson, M. Hencz, A. Szakács, et al.. Growth and erosion rates of the East Carpathians volcanoes constrained by numerical models: Tectonic and climatic implications. *Geomorphology*, 2020, 368, pp.107352 (IF 3,819). 10.1016/j.geomorph.2020.107352 . hal-02926347

HAL Id: hal-02926347

<https://hal.science/hal-02926347>

Submitted on 22 Aug 2022

HAL is a multi-disciplinary open access archive for the deposit and dissemination of scientific research documents, whether they are published or not. The documents may come from teaching and research institutions in France or abroad, or from public or private research centers.

L'archive ouverte pluridisciplinaire **HAL**, est destinée au dépôt et à la diffusion de documents scientifiques de niveau recherche, publiés ou non, émanant des établissements d'enseignement et de recherche français ou étrangers, des laboratoires publics ou privés.



Distributed under a Creative Commons Attribution - NonCommercial 4.0 International License

Growth and erosion rates of the East Carpathians volcanoes constrained by numerical models: tectonic and climatic implications

**Dibacto, S.¹, Lahitte, P.¹, Karátson, D.², Hencz, M.², Szakács, A.³, Biró, T.², Kovács, I.⁴,
Veres, D.⁵**

¹GEOPS, Univ. Paris-Sud, CNRS, Université Paris-Saclay, Rue du Belvédère, Bât. 504, 91405
Orsay, France

²Eötvös University, Department of Physical Geography, H-1117 Budapest, Pázmány s. 1/C,
Hungary

³Department of Environmental Sciences, Sapiientia University, Calea Turzii nr. 4, 400193 Cluj
Napoca, Romania

⁴Geological and Geophysical Institute of Hungary, Geochemical and Laboratory Department,
Stefánia út 14, 1143 Budapest, Hungary

⁵Institute of Speleology, Romanian Academy, Clinicilor 5, 400006 Cluj-Napoca, Romania

Abstract

The East Carpathian volcanic range experienced an along-arc, Late Miocene to Quaternary migration of eruptive activity during its ~11Ma-long activity. Here, a novel and complex methodology is presented that yields new geochronological and geomorphological constraints on the evolution of the 20 volcanic edifices. New unspiked K-Ar ages either constrain their lifespan (6.79±0.10 - 6.47±0.09 Ma for Seaca-Tătarca; 5.47±0.08 - 4.61±0.07 Ma for Vârghiș) or date the youngest volcanic activity (central Călimani). In parallel,

numerical reconstructions of volcanic paleo-topographies were performed to quantify their shape at the end of their construction stage. The inferred initial volcano size shows a wide range (3 to 592 km³), making up the four main successive volcanic segments (910, 880, 279 and 165 km³ for Călimani, Gurghiu, North Harghita and South Harghita segment, respectively) totalizing 2200 km³ and an average growth rate of 200 km³/Ma at range-scale. At the volcano-scale, with only consideration to their respective time spans (i.e. avoiding repose periods), growth rate is characterized by two major trends: a moderate growth rate (137 km³/Ma) for the older volcanoes (11-3.6 Ma) followed by a lower growth rate (28 km³/Ma) obtained for the Plio-Quaternary volcanoes. Comparing reconstructed and current topographies yielded a total eroded volume of 524±125 km³, defining averaged denudation of 22% and a 20 m/Ma erosion rate. Erosion rates for major climatic periods were computed, which highlight the contrasting climatic contexts since 11 Ma. The highest erosion rate (38 m/Ma) occurred during transitional moderate subtropical-continental climate period (9.5-8.2 Ma). An intermediate erosion rate (14 m/Ma) characterized a moderate continental climate period (8.2-6.8 Ma) when conditions became less humid. The lowest erosion rate (7 m/Ma) reflects the prevailing continental but occasionally semi-arid climate (6.8-5.8 Ma). The highest erosion rate (28 m/Ma) was obtained for Plio-Quaternary times during the interglacial/glacial cycles. Such a quantitative morphometric and geochronological approach demonstrates its efficiency to study volcanic dynamism, including both constructional and erosional processes, through time.

Keywords

Numerical reconstruction; Volcano growth; Erosion rate; Paleo-climatic constraint

1 Introduction

A major geomorphological approach consists in assessing the time-dependent evolution of paleo and present topographies of landforms alongside the geological processes involved in their genesis, and, if possible, in numerically quantifying such processes (Leverington et al., 2002; Persson et al., 2004; Székely and Karátson, 2004; Wright et al., 2006; Grosse et al., 2009; Tucker and Hancock, 2010; Grosse et al., 2012; Karátson et al., 2012; Lahitte et al., 2012; Salvany et al., 2012). In volcanic fields with readily dateable topographic surfaces, one can constrain both dynamisms of volcanic growth and degrees of dismantling. Obviously, short-lived, recent, well datable volcanoes (i.e. of Late Quaternary age) can be studied with a high level of precision, whereas for older systems the precision will decrease. Growth and destruction of volcanoes may or may not be coupled, controlled by either endogenic (tectonic forces, volcanic eruptions) or exogenic processes (erosion controlled by climatic factors) (Thouret, 1999). A number of studies have aimed at constraining the total long-term erosion of volcanic surfaces using two approaches: 1) investigate long-lived but steady sourced volcanic systems such as stratovolcanoes based on edifice changes to track long-term erosional processes (Hildenbrand et al., 2008; Germa et al., 2011; Lahitte et al., 2012; Karátson et al., 2012; Salvany et al., 2012; Ricci et al., 2015a); and 2) study short-lived but dispersed small volcanic systems such as monogenetic volcanic fields using individual point-like data to extrapolate and understand the entire field behaviour (Kereszturi et al., 2013; Blaikie et al., 2015; Grosse et al., 2018). However, in the case of active volcanoes (with current eruption), a mass balance can be carried out either by quantifying the evolution of the topography of the volcano before, after, during and after the eruption or by carrying out a balance of the sediment load which is then reported on the surface of the watershed (Thouret et al., 2014). Digital elevation models (DEM) allow for characterizing the patterns of

erosion, and to extract geomorphic and structural information on large-volume edifices which cannot be easily studied in the field (Favalli et al., 1999; Székely and Karátson, 2004). DEM-based quantitative geomorphological investigations enable the calculation of constructed and/or eroded volumes and thus estimate magma output as well as erosion rates. These, in turn, can be linked to hydroclimate variability driving the long-term erosion processes: in the Carpathians, a humid continental climate (Karátson and Timár, 2005; Karátson et al., 2019); in other areas with tropical and/or arid climates (Le Friant et al., 2004; Samper et al., 2007; Hildenbrand et al., 2008; Germa et al., 2010, 2015; Karátson et al., 2012; Lahitte et al., 2012; Salvany et al., 2012; Ricci et al., 2015a, 2015b; Bablon et al., 2018).

This study combines new geochronological constraints with a quantitative geomorphological overview of the Călimani-Gurghiu-Harghita¹ volcanic range (hereafter CGH, Fig. 1) in order to decipher its long-term topographic evolution. The unspiked Cassinol-Gillot K-Ar technique has been used to obtain precise ages on four of the 17 volcanic centres (Central Călimani, Seaca-Tătarca, Vârghiş and Pilişca volcano). Also, we performed DEM analysis to numerically model the paleo-topography of the volcanoes by computing the best fitting surface to the volcanoes, making it possible to obtain constructed and eroded volumes. Combining geomorphological information with available geochronological data allow us to accurately assess the geomorphic evolution by calculating growth and erosion rates, which in turn help constrain the timing and dynamism of magmatic processes and to investigate links between tectonic and magmatic dynamism (Wadge, 1982, 1984; Grosse et al., 2018).

¹ Official Romanian names are completed by locally used Hungarian names in Tables, also helpful for the reader to find names on local maps.

From cumulative erosion rates, computed at the scale of each volcano, we investigate their variations and how they correlate to the main climatic fluctuations under variegated but temperate continental climate-dominated conditions (Karátson, 1996), that the CGH area has experienced since the onset of volcanism started at 10.6 Ma (Pécskay et al., 1995).

2 Geological setting

The Carpathians are a major mountain range in Central and Eastern Europe spanning from Eastern Bohemia (Czech Republic), Poland, Slovakia, Hungary, Ukraine, to Romania and Serbia. Linked to the Alpine and Dinaric systems, they encompass the Pannonian and Transylvanian Basins (inset Fig. 1). Volcanic activity related to complex Tertiary to Quaternary geodynamic processes occurred both along the inner part of the Carpathian orogen and in the Carpatho-Pannonian Basin (Rădulescu and Săndulescu, 1973; Csontos et al., 1992; Szabó et al., 1992; Seghedi, 1995; Mason et al., 1996, 1998; Seghedi et al., 1998, 2004a, 2004b, 2005a, 2005b; Fielitz and Seghedi, 2005; Seghedi et al., 2019).

Located in the eastern part of Romania's Inner Carpathians, the 160 km long CGH volcanic range constitutes the youngest, longest and southeasternmost segment of the Carpathian volcanic range (Fig. 1). The CGH is a typical post-collisional volcanic range as it developed after the stacking of the collision-related East Carpathian nappe system (Matenco and Bertotti, 2000). After the collision and the step-by-step propagation of the CGH volcanism parallel with the orogen, the plate boundaries more or less sealed. It was assumed to be associated with asthenosphere upwelling, explained by progressive break-off of an assumed Miocene subducted slab (Mason et al., 1998; Seghedi et al., 1998), as suggested by the present high heat flow coinciding exclusively with the volcanic area (Tari et al., 1999; Demetrescu et al., 2001). The CGH consists of a NW–SE-trending row of several adjoining

and partially overlapping volcanoes mostly characterized as composite volcanoes in the axial part and resulting from complex eruptive histories, including several cone-building phases interrupted by destruction phases (Szakács and Seghedi, 1995). The subduction-related, post-collisional volcanism (Rădulescu and Săndulescu, 1973; Pécskay et al., 1995; Seghedi et al., 2004a; Lexa et al., 2010) resulted in products which display calc-alkaline to alkaline compositions with andesite-dominated rock types (Mason et al., 1996, 1998; Seghedi et al., 2011). Volcanism of the overall CGH segment was interpreted as coeval with the last peak of crustal deformation in the Carpathian bend zone, characterized by uplift in the orogenic zone and subsidence in the foreland with amplitudes in the order of 2-4 km (Matenco et al., 2010).

3 Volcanism of the CGH range and its timing

The CGH volcanic range divides into four sub-segments corresponding respectively from the north to south to Călimani, Gurghiu, Northern and Southern Harghita (Fig. 1). As a result of the migration of volcanic activity along the range, the overlap between its 17 eruption centres is limited, allowing one to individualize them quite well. The first comprehensive study of CGH (Szakács and Seghedi, 1995, 1996) pointed out the systematic decrease of volume, height and width of the volcanic edifices from north (Călimani) to south (Southern Harghita), most of them surrounded by extended and partly coalesced volcanoclastic aprons.

The pre-volcanic basement of the CGH volcanic range belongs to two different major tectonic units, lithologically characterized by Proterozoic to Lower Palaeozoic metamorphic rocks overlain by Mesozoic, mostly carbonatic, sedimentary rocks of the East Carpathian's "Crystalline-Mesozoic Zone" in the eastern part (Săndulescu, 1988). A thick Paleogene-Neogene sedimentary pile including ductile rocks such as clay and salt prone to plastic

deformation (Ciupagea et al., 1970; Szakács and Krézsek, 2006) forms the pre-volcanic basement in the western part along the rim of the Transylvanian Basin. A topographic “anomaly” consisting in reverse-dipping (i.e. towards volcano center instead of towards volcano periphery) of the peripheral outer slopes of some volcanoes (e.g. Făncel-Lâpușna and Seaca-Tătarca in Gurghiu Mts, and Vârghiș volcano in North Harghita, Fig. 1) was interpreted by Szakács and Krézsek (2006) as resulting from complex interactions between the pre-volcanic basement and the overlying volcanic edifices. Namely, the Late Miocene volcanoes grew up on a pre-volcanic basement including a thick salt layer which was squeezed-out, displaced and involved in enhanced diapirism governed by gravitational effects of the volcano loading. These processes modified in a certain degree also the original volcanic topography by volcano spreading (Delaney, 1992; Borgia, 1994; Merle and Borgia, 1996; Lagabriele et al., 2000; Wooller et al., 2004; Borgia et al., 2005; Grosse et al., 2009, 2012), namely increasing edifice diameter and reducing relative height differences between volcano centre and periphery, hence reducing relief energy and erosion rates.

Available ages along the CGH range (Peltz et al., 1987; Szakács et al., 1993; Pécskay et al., 1995, 2006; Seghedi et al., 2004b, 2005; Karátson et al., 2019; Lahitte et al., 2019) defined a quasi-continuous eruptive activity from 10.6 to 0.03 Ma. The southwardly shift in eruption centres has been linked to progressive slab detachment following an oblique subduction stage (Mason et al., 1998; Seghedi et al., 1998).

For the past 10.6 Ma, the CGH range has been experiencing a temperate subtropical-continental climate with occasionally arid periods in the Late Miocene and a relatively humid climate with occasional periglacial regimes and interglacial/glacial variability during the Pliocene and Quaternary (Karátson, 1996; Fielitz and Seghedi, 2005; Magyari et al., 2014).

Details and evidence concerning climate changes in the Carpathian area are given in the discussion.

4 Methods

4.1 K-Ar ages by unspiked Cassinol–Gillot technique

Seventeen new groundmass K-Ar ages are first presented here (Table 1). Results were obtained on samples collected from four volcanoes representing the three main sectors of the range (Călimani, Gurghiu, North and South Harghita). Measurements followed the protocol of rock sampling, preparation and measurement as described by Germa et al. (2011) and detailed in the supplementary materials (S.M.).

4.2 DEM-based volume calculations

Using a quantitative DEM-based approach of volumetry (Székely and Karátson, 2004; Karátson and Timár, 2005; Favalli et al., 2009; Grosse et al., 2009; Kervyn et al., 2012; Lahitte et al., 2012; Lavigne et al., 2013; Karátson et al., 2013; Germa et al., 2015; Ricci et al., 2015a), we numerically modelled the paleo-topographies of all CGH volcanoes. To constrain the shape that they displayed directly after the end of their respective activity, we follow the method introduced by Lahitte et al. (2012) and improved since by Germa et al. (2015). The resultant modelled volcanic surfaces are used to assess constructed and eroded volumes (Ricci et al., 2015a), and then, using the available chronological data, to constrain the time-space dynamism of volcano surface evolution through both construction and erosion rates. To achieve our objectives, the topography of the CGH volcanic range was analysed from the Shuttle Radar Topography Mission (SRTM) 30m-resolution DEM. Topographic surfaces were modelled at 100m-resolution that compromises sufficient details of reconstruction and time

of calculation without affecting their quality (Wright et al., 2006; Grosse et al., 2009; Karátson et al., 2010; Kervyn et al., 2012).

4.2.1 Volcanic paleo-surface model

The main body of work relates to the topographic reconstruction of a volcano, i.e. the modelling of the surface that it reached after its growth ceased (the so-called pre-erosional volcanic surface, or PEVS). To model such surfaces, we use as input data the sectors of the current topography that still testify to the PEVS or, in other words, that have undergone ideally zero or minimal erosion since the volcano construction ceased. In detail, each grid cell of the present-day DEM was converted in a XYZ point, forming a huge input database (20 million points). Next, different morphometric parameters such as slope, topographic position index (TPI, Weiss, 2001) and topographic openness (TO, Yokoyama et al., 2002; Favalli and Fornaciai, 2017) were computed, assigned as attributes for each point and combined to select only points belonging to PEVS. These so-called constraining points (CPs) are commonly located on quasi-planar surfaces found commonly in the mid- to lower flanks of the volcanoes which, during long-term erosion, tend to be preserved relatively to the upper flanks and central parts that encompassed central depressions (Karátson et al., 2016; Favalli and Fornaciai, 2017). More than 200,000 CPs for the entire CGH volcanic range (Fig. 2A) were extracted. For practical reasons, they were reduced to one tenth without breaking the homogeneity of their distribution. The Seaca-Tătarca volcano (06 in Fig. 1) example is shown in Figure 3 to illustrate CPs extraction (purple dots in Fig. 2A, Fig. 3A and Fig. 3C) from its whole surface (green dots in Fig. 3A and coloured surface in Fig. 3C) and in consideration to slope, exposition, TO and TPI parameters. The elevation versus distance to centre diagram (Fig. 3A) highlights how CPs, independently of their position along the volcano profile (lower, mid or upper), belong to planezes surfaces, i.e. to the locally (at hundred-meter scale)

uppermost surface of the volcano. Note that only the main edifice was selected without considering the volcanoclastic materials of the ring plain immediately surrounding the central edifice (Zernack et al., 2011; Németh and Palmer, 2019). Finally, a careful visual control has been carried out in order to remove outlier points accidentally present in the ultimate CPs database. From their respective CPs, numerical reconstructions of 15 from the 16 selected volcanoes have been modelled using the ShapeVolc (SV) algorithm (Lahitte et al., 2012). Only Pilişca volcano (a small-sized shield volcano topped by a few lava domes in South Harghita; Szakács and Seghedi, 1995) has been reconstructed by the Kriging interpolation (Krige, 1951).

The ShapeVolc algorithm dedicated to volcano surface modelling was used successfully in various dismantling contexts: large flank collapse (Lahitte et al., 2012; Germa et al., 2015), caldera formation (Lavigne et al., 2013) or regressive erosion (Salvany et al., 2012; Ricci et al., 2015a, 2015b). This algorithm, as well as the one proposed by Favalli et al. (2014), fit the ideal surface by minimizing the mean square error between this surface elevation and those of the CPs.

ShapeVolc algorithm, assuming that a volcano displays at first order an axial symmetry (Karátson et al., 2012), finds, using the simplex algorithm, the set of parameters that define the first order geometry of a volume defined by a surface of revolution. Adjusted parameters are: XYZ coordinates of the axis of revolution (the location and elevation of the vent/summit); the elliptical shape of the edifice (i.e. the shape of its contour lines); and the parameters of the generatrix of the surface revolution (i.e. the function, black dots in Fig. 3B, that best fit the non-eroded upper volcanic surface). As the current elevation of each CPs is the lowest one possible for the uppermost surface, parameters are calculated in order to

find the lowest possible surface of revolution passing above most of the CPs (see black curve relatively to purple dots in Fig. 3A).

A common way to model volcano shape and volume consists in a simple rotation of the best generatrix curve around an axis located at the volcano summit, defining a pure surface of revolution (Karátson et al., 2010, 2012). However, such kind of modelling does not consider the ellipticity of the volcano that is a common characteristic of edifices (Grosse et al., 2012, 2014; Favalli et al. 2014; Grosse and Kervyn, 2018). The observed improvement of results, when ellipticity is considered advocate for closely considering volcano eccentricity in our reconstructions (see details given in S.M.), has been done in this study: eccentricity and azimuth have been systematically computed.

Moreover, as taking into account the volcanic complexity of the surface is crucial to optimize precision in volume calculation, a major improvement is here introduced to allow ShapeVolc to take into account the second order of magnitude of details of volcanic surfaces. Indeed, if most volcanoes can be defined at first order by a mathematically defined, elliptical surface of revolution, the complexity of volcanic construction introduces heterogeneities on this mathematic perfection that commands modelling the second order of magnitude of their shape. Concretely, each PEVS model was performed in two steps. 1) The first order of magnitude of the volcanic surface was obtained by defining the unique set of parameters (listed above) that best fit to all CPs of the volcano. 2) The second step locally adjusts the surface to find elevation of each cell of the 100 m-resolution paleo-surface model with only considering the closest CPs of the given cell and selected by classical research criteria (typically the 20 nearest CPs in each of the eight 45°-large angular sectors). This time-consuming step (up to 120,000 elevation points to be modelled for a large volcano) allows for defining the uppermost PEVS and takes into account the irregularities of

the surface such as local elevation variations and small details in the volcanic structure (presence of parasitic and/or adventive cones or domes, such as Tarvez in Fig. 3A). This second order of detail becomes essential for young volcanoes where the very small amount of erosion material imposes the most adjusted surface as possible.

Uncertainty of our modelled volcano shapes (σZ_{SV} , Table 2) is calculated as the standard deviation of the difference (ΔZ_P) between the altitude of the constraining points (Z_{CP}) and the altitude of the modelled ones (Z_{SV}).

4.2.2 Volumetric data, growth and erosion rates

Estimating the volcano volume requires knowing the surface of its basement prior to its construction, the so-called pre-volcanic basal surface (PVBS). Details of PVBS modelling by kriging interpolation are given in the S.M.

Comparisons of pre-erosional volcano surface to PVBS and the present DEM allow calculations of constructed (V_C) or eroded (V_E) volumes, respectively. Next, the growth rates (GR, in km^3/Ma) defined by V_C divided by volcano lifespan (Δt) constrains the eruptive dynamism; the erosion rate (ER, in m/Ma) defined by V_E divided by the area and the erosion duration (i.e.; volcano age) and the degree of denudation (D_{Den} , the percentage of volcano volume removed by erosion), defined by V_E divided by V_C , are computed. Details of the modelling of PVBS and calculation of volumes and uncertainties, degree of denudation, growth and erosion rates are given in the S.M. The inferred erosion is highlighted in Fig. 3C by the black sticks that connect the present DEM as well as the PEVS surfaces.

Our reconstructions include both coherent and fragmented volcanic materials making up the edifices, and thus, they refer to bulk volumes instead of DRE (dense rock equivalent). Our constructed volumes and growth rates take into account the volcanoclastic aprons, but they are excluded from the V_E and ER since our calculations do not differentiate the

volcaniclastic aprons (their source and to which volcano they belong); so, an accurate proportioning is quasi-impossible. Our volcano GR differs from magma output rates sensu stricto as they only integrate a part of the whole pyroclastic material. However, it allows the obtaining of a general framework of magmatic activity through space and time along the CGH range and can be used as a good proxy for magma output rates (Wadge, 1982, 1984; Grosse et al., 2018).

5 Results

5.1 K-Ar ages

New K-Ar ages are reported in Table 1, with all uncertainties quoted at 1-sigma level (1σ). All Ar analyses were successfully duplicated at the 1σ level except sample 17EC14 that required a third measurement (see details of each measurement in the S.M.). Radiometric dating results are presented in chronological order in the following sections, compiled in Table 1 and discussed in Fig. 2A-D.

5.1.1 Călimani edifice

The four oldest dated samples of lava flows and intrusions belong to the Călimani caldera edifice. The oldest ages (8.30 ± 0.12 and 8.33 ± 0.12 Ma) were obtained on two distinct outcrops from the same andesite lava flow, illustrating the good reproducibility of our dating method. The monzodioritic intrusion exposed in the central part of the Călimani caldera is slightly younger (8.26 ± 0.12 Ma). In contrast, the dacitic lava dome at Pietricelul, built up on the Călimani caldera rim, constrains the post-caldera activity (6.69 ± 0.10 Ma) and is comparable with the youngest ages measured previously in the Călimani area (Pécskay et al., 1995).

5.1.2 Seaca-Tătarca volcano (Gurghiu Mts.)

Five andesitic lava flows were dated on this large lava dominated volcano. Stratigraphical coherence is observed, as the oldest ages have been obtained on the innermost and lowest samples (6.65 ± 0.09 and 6.79 ± 0.10 Ma). Two intermediate ages were obtained from lava flows on the upper flanks of the volcano on the SSE and western sides (6.61 ± 0.09 and 6.52 ± 0.09 Ma, respectively). The youngest age was obtained on the uppermost rim of the erosional depression (6.47 ± 0.09 Ma) in accordance with the relative stratigraphy. From the dated samples (that likely constrain the whole Seaca-Tătarca volcano stratigraphy), we infer a constructional period of $\sim 330 \pm 140$ ka.

5.1.3 Vârghiș volcano (North Harghita Mts.)

From the six andesite lava flows dated on the Vârghiș volcano, the oldest age (5.47 ± 0.08 Ma) has been obtained on the only amphibole lava located in the lowest outcrop of the north sector of the central depression (identified as a sector-collapse depression by (Szakács and Seghedi, 1995, 2000). Two lava flows sampled inside the depression have provided intermediate ages (5.06 ± 0.07 and 4.79 ± 0.07 Ma) whereas two other (4.65 ± 0.07 and 4.89 ± 0.07 Ma) came from the upper flank of Harghita Mădăraș summit, described as a depression rim dome (Szakács and Seghedi, 1995). Finally, the post sector collapse and youngest activity is constrained at the southern periphery of the edifice (4.61 ± 0.07 Ma). From these ages, we infer a constructional period of $\sim 900 \pm 140$ ka.

5.1.4 Pilișca volcano (South Harghita)

Two dacitic lava rocks from the Pilișca volcano (1.98 ± 0.06 and 2.11 ± 0.04 Ma) might represent late-stage dacitic lava domes stratigraphically overlying andesitic lavas of the early volcano stage located along the riverbed of the Olt river in the Tușnad Gorge (2.11 ± 0.03 and 2.13 ± 0.03 Ma, in Karátson et al. 2019).

5.2 Volcanic surface models

5.2.1 Paleo-volcanic surfaces

From their constraining points (Fig. 2A), 16 CGH volcanoes were modelled (Fig. 4). Their morphometric characteristics are summarized in Table 2 (more exhaustively discussed in S.M.). They display two types of radial profile according to their main concave (modelled by an exponential or polynomial curve) or convex (gaussian curve) shape (Grosse et al., 2009). Ellipticity ranges from 0.16 (quasi-circular edifice) to 0.80 (strongly elongated one). Uncertainties of modelled surfaces range from 24 m to 82 m. Modelled volcanoes are characterized by contrasting sizes, from very small parasitic cones (Râchitis edifice, #12, 3 ± 3 km³) to large composite volcanoes (Central Călimani edifice, #01, 592 ± 115 km³; Fig. 1 and Fig. 4).

In the Călimani sector (Fig. 4A), the Central Călimani (#01, constituted by the current S and SE flanks of Rusca-Tihu and the associated cones of Lucaciul and Tămău) and Moldovanul (#02) edifices have been reconstructed. They display contrasting shapes; the quasi-circular Central Călimani is best fitted by a concave shape (steep summit) whereas the more elliptical Moldovanul fits to a convex shape (relatively flat summit).

For Gurghiu sector (Fig. 4B), seven volcanoes have been modelled (#03 to #09, Fig. 4B). Whereas all have quite similar concave shape, four volcanoes (#03, #04, #05, #08) exhibit relatively high ellipticity (0.61-0.80) whereas the others are almost circular (0.16-0.37).

In North Harghita, all four modelled volcanoes (#10 to #13, Fig. 4C) display a marked ellipticity (0.33-0.80) and concave shape, except the very small Râchitis with a convex profile.

In South Harghita (Fig. 4D), the dual Luci-Lazu (#14a and #14b) and Cucu (#15) volcanoes display contrasting ellipticity (0.20 and 0.49, respectively) but both with quasi-linear profiles

(almost conical shape). Pilișca (#16), the youngest volcano in our study (only the late Pleistocene Ciomadul is younger in the whole CGH, Szakács and Seghedi, 1995; Karátson et al., 2019; Lahitte et al., 2019), has a such “un-geometric” shape that it requires kriging interpolation.

5.2.2 Volumetric results

Using the output from the geomorphological models, the main individual data for each volcano are compiled in Table 2 and comprise the area (A), Height, constructed (V_c) and eroded (V_E) volumes, growth (GR) and erosion (ER) rates and the degree of denudation (D_{Den}). To compute GR and ER, we considered all available radiometric ages from previous studies, most remaining conventional K-Ar ages being obtained on whole rock. For each volcano, we calculated an average age using as bracketing temporal constraints the oldest and youngest available ages and assuming that the average age represents the peak of activity.

The V_c computed for the 16 volcanoes modelled in this study ranges between 3 ± 3 and $592 \pm 190 \text{ km}^3$. Fitting the volcano volume and area by a power-law function shows a good positive correlation ($R^2=0.93$; Fig. 5A) defined by:

$$V_c = 0.015 \times (A)^{1.51} \quad \text{Eq. 1}$$

We note that data on Fâncel-Lăpușna (in Gurghiu) seems out of this general trend; however, its inclusion or exclusion from the analysis practically does not alter the correlation (R^2 remains 0.93). Dimensional analysis shows that volume and surface are related by a power-law function with a 1.5 exponent. For instance, a regular cone (radius R, height H, slope α) is defined as:

$$V = \tan(\alpha) / (3 \times \pi^{1/2}) \times A^{1.5} \quad \text{Eq. 2}$$

Using the computed volume and area of the 16 analysed volcanoes (some showing very irregular shapes due to emplacement above or around older ones and having different shapes, all displaying second order of magnitude, i.e. not a simple mathematical shape), we obtained roughly the same 1.5 correlation exponent between the two variables (Fig. 5A). We interpret this quasi-ideal correlation as the expression that, although each volcano experienced its own history of construction, the individual long-term growth was averaged out as a quite similar and common evolution along the range. Such a quantification approach, based on enhanced morphometry, can be considered as numerical validation of the trend predicted for arc volcanoes evolving from single cone to massif (Grosse et al., 2009).

Plotting the height versus volume diagram as proposed by Grosse et al. (2009) (Fig. 5A inset), they fall in the field of the massif trend which is coherent with the complexities of their topography and eruptive history. Furthermore, the power-law curve fitting CGH data in the height versus volume diagram (Fig. 5A inset) has a power exponent close to $1/3$ (0.35). Again, this means, inverting the equation, that volume is almost related to height by a factor of three and confirms the more and less homomorphic shapes of all CGH volcanoes.

The V_E computed in this study ranges between 0.2 km^3 (Ciomadul) and $158 \pm 85 \text{ km}^3$ (Călimani), increasing toward the north of the range with ER range between 7 and 26 m/Ma. The degree of denudation of the studied volcanoes is in the range of 3–34% (the average weighted mean being 22%), which means that within the studied period ($\sim 11 \text{ Ma}$), less than one third of the original volcanic edifice has been removed by erosion.

Plotting the V_C against V_E shows a strong linear positive correlation with $R^2=0.95$ (black line, Fig. 5B) whereas D_{Den} values (expressed as percentages in Fig. 5B) do not systematically

fit with the V_C , i.e. small edifices (e.g. Bacta, Jirca, Moldovanul), as well as large ones (Călimani, Fâncel-Lăpușna) can display a high degree of denudation.

No correlation ($r^2=0.01$) exists between the degree of denudation (D_{Den}) and height (H) (Fig. 6A) and, logically, with volume or area as they are strongly correlated. Additionally, no effect on erosion by any altitudinal contrast appears. On the other hand, D_{Den} fit relatively well with latitude ($R^2=0.62$, Fig. 6B). As morphometry of volcanoes cannot explain this fit, other parameters such as age, spatial climate fluctuation, rock strength and edifice slope can possibly drive this regional variation of the D_{Den} values. These aspects will be further addressed in the discussion.

6 Discussion

6.1 Volume comparison with previous results

Summarizing individually modelled constructional volumes (i.e. prior to erosion) leads to a total original volcanic volume of $2240\pm190\text{ km}^3$ in the CGH range during $\sim 11\text{ Ma}$, higher than the $1400\text{--}1606\text{ km}^3$ range previously proposed (Szakács et al., 1997; Karátson and Timár, 2005; Seghedi et al., 2019) obtained with basic approaches. We interpret this higher value compared to previous studies as due to the complete integration of erosionally removed volumes over the whole edifice. Hence, our approach illustrates the importance of reconstructing a full paleo-topography of the volcanic edifice, especially for heavily dismantled volcanoes such as those in the Călimani and Gurghiu segment.

A clear anticorrelation exists between relative uncertainties of constructed volume (σ_{RELV_C} , range from 19% to 50%, details in S.M.) and average height (ΔH_{mean} , Fig. 7) and fits particularly well ($R^2=0.87$) to an inverse function. Even if calculation of relative uncertainty is

obtained from a complex integration of elementary uncertainties over the whole area of the volcano, it can be approximated as

$$\sigma_{\text{RELV}_C} \approx \sqrt{(\sigma_{\text{Mean_upper_surface}}^2 + \sigma_{\text{Mean_lower_surface}}^2)} / \Delta H_{\text{mean}} \quad \text{Eq. 3}$$

where, ΔH_{mean} is the average elevation of the edifice, and both σ_{Mean} terms are the average uncertainties of the basal and upper surfaces. Consequently, for a given volume, the smaller the ΔH_{mean} , the more poorly constrained its average height, and the higher, the relative uncertainty associated to its reconstructed volume (σ_{RELV_C}).

6.2 K-Ar age constraints

6.2.1 Comparison with previous radiometric age data

All new K-Ar ages (obtained on Central Călimani, Seaca-Tătarca, Vârghiș and Pilișca volcanoes, Table 1, Fig. 2A-D) match within 1σ with the previous, respective conventional K-Ar ages. As such, the main issue is not necessarily the absolute values but, rather, improving their precision, since the uncertainty has been reduced by a factor of 3 to 5 (typically around 0.1 Ma vs 0.4 Ma). This improvement is crucial for correctly defining the dynamism of the volcanism, which requires precise constraints on volcano lifespans.

The lifespan of Seaca-Tătarca volcano, for example, is shortened from a previous estimate of 1 ± 0.4 Ma (Pécskay et al., 1995; Seghedi et al., 2004b) to 340 ± 140 ka. For Vârghiș volcano, the new results slightly extend its youngest activity (4.61 ± 0.07 Ma, this work, vs 4.9 Ma in Pécskay et al., 1995) and refine its relatively long lifespan from 0.7 ± 0.4 to 0.9 ± 0.1 Ma. For Pilișca volcano, newly dated units do not sufficiently encompass its full activity to allow constraining its lifespan based only on the new K-Ar ages.

6.2.2 Example of volcano growth through time: The case of Seaca-Tătarca volcano

The study of the well-defined, regular-shaped simple edifice of Seaca-Tătarca benefits from regularly distributed, well-dated samples, allowing for precisely correlating its volume growth rate through time (Fig. 8A and Fig. 8B), and proposes a growth model encompassing its whole construction phase. For this purpose, the dated samples are projected in a graph of elevation versus distance to centre, with correction of the ellipticity of the edifice (Fig. 8A). Next, considering the average topographic profile of the volcano at the end of its construction and assuming a homothetic construction (i.e. shape remains self-similar all the time), we computed the proportion of the volcano volume that was already constructed with constant growth rate when subsequent, dated lava flows erupted.

Based on this, the location of the oldest sample (17EC03) is calculated as corresponding to 10% of the construction of the edifice (Fig. 8A) which is consistent with its outcrop in the large, central erosive depression that has not yet sufficiently dismantled the innermost part of the volcano to reach its basement. Though coming from a lower elevation than the previous one, sample 17EC04, belongs to an upper section of the volcano (21% of the construction). It outcrops in a river valley whose topographic profile (represented by the lowest green dots in Fig. 8A) is less sloping than the volcanic sequence it crosscuts. Consequently, outcrops along this valley display younger and younger volcanic units toward the periphery of the volcano. Sample 17EC05 corresponds to an intermediate position during the construction of the edifice (65%) despite its location in the upper flanks. Indeed, as the volcano grew, its area increased, too, requiring more and more material to increase its elevation. Consequently, each new % of growth (i.e. elevation) occupied progressively lower thicknesses (in Fig. 8A, blue lines regularly spaced at 10% are closer and closer upward). The

uppermost and youngest dated lava flows (17EC02 and 17EC01, Fig. 8A) correspond almost to the last stage of the edifice construction (92% and 95%, respectively).

From these growth proportions through time (white dots in Fig. 8B), and assuming magma output rate as constant (straight line in Fig. 8B), we can define the growth pattern of the whole volcano. In particular, the age of the onset and end of its activity can be inferred as the time interval where the growth line intersects 0% and 100% of growth proportions, respectively. With consideration of uncertainties, this interpolation leads to a full construction of Seaca-Tătarca volcano from 6.80 Ma to 6.46 Ma (red dots in Fig. 8B) and, consequently, a lifespan of ~340 ka. Based on such detailed findings of a selected volcanic edifice, we can assume that detailed chronological studies on similar-sized volcanoes along CGH would result in faster growth rates as well.

6.3 Spatio-temporal evolution of the CGH volcanism

Compiling all available K-Ar ages (Fig. 9), i.e. the new unspiked K-Ar ages along with those on Ciomadul and Pilișca and the numerous conventional K-Ar ages, the previously recognized diachronism in volcanic activity along the CGH range can be confirmed, generally characterized by decreasing ages southward from the late Miocene (~ 11 Ma) volcanism in Călimani to the sub-recent (<0.1 Ma) activity at Ciomadul (Rădulescu and Săndulescu, 1973; Peltz et al., 1987; Szakács et al., 1993, 2018; Pécskay et al., 1995, 2006; Seghedi et al., 2004b; Seghedi et al., 2005; Karátson et al., 2019; Lahitte et al., 2019). However, detailed analysis along the range highlights overlaps in volcanic activity between some segments. In particular, the activity of Călimani and Gurghiu was partially simultaneous, roughly between 9.8 to 6.3 Ma (Seghedi et al., 2004b, 2005b; Pécskay et al., 2006). A second overlap is observed between the latest activity in Gurghiu and the early activity of North Harghita (6.3 - 5.1 Ma).

Detailed observation of southward age progression along the CGH range allows for observing various compartments in each segment (Fig. 9). For Călimani, volcanic activity was coeval in both edifices (Central Călimani and Moldovanul), the earliest activities starting in the northern area and then shifting southwards. This mechanism is highlighted by the trapezoid box in Fig. 9 illustrating how early activity started only in the north but subsequently took place simultaneously in the entire segment. In Gurghiu, also, southward age progression does not establish a real migration, but, instead, an extension of the volcanically active area (green trapezoid in Fig. 9). Isolating the oldest Gurghiu ages for each 20 km-large windows allows constraining its southward expansion (black line on Fig. 9). Starting from only Jirca's activity at the beginning, the volcanism experienced a widespread expansion of activity at a rate of 12.6 km/Ma ($R^2=0.75$) over the whole segment (all volcanic centres being active quasi contemporaneously). It seems that during this period, the volcanism reached its paroxysm and accounted for the main activity apparent at around 6.6 Ma (Fig. 10).

On the contrary, volcanism in North and South Harghita shows a well-defined southward migration. A full progression of ages can be observed toward the south, as activity in each subsequent volcanic centre generally begins at a progressively later date with relatively good correlations. Between 6.3 and 4.6 Ma, volcanism migrated at a rate of 13.4 km/Ma ($R^2=0.72$) over the whole North Harghita segment. Subsequently, from 4.3 to 0.03 Ma, volcanism continued to progress southward along South Harghita. Samples obtained for each volcanic centre show a narrow age range (typically <1 Ma), reflecting the migration of activity but at a slower rate (4.6 km/Ma, $R^2=0.68$; Fig. 9) than along the older parts of the CGH.

6.4 Growth rates evolution through time and tectonic implications

Combining ages with the new volume constraints allows for characterizing the major phases of volcanic activity, the quiescence periods and the evolution of magma output (Fig. 10A). To quantify this, the volume of each volcano is assumed to be erupted between the youngest and the oldest available ages, with a maximum output occurring at half-time of the age range (Grosse et al., 2018) and individual GR through time is defined, at volcano-scale, by a Gaussian-like curve (coloured curves in Fig. 10A). Next, summing all individual outputs through time, we computed cumulative growth rate (dashed grey line in Fig. 10A). Finally, the derivation of this curve gives the GR through time for the whole CGH volcanic activity (bold line in Fig. 10A). Even though the regional GR does not consider the possible subvolcanic bodies (see discussion in Karátson and Timár, (2005), it remains a good proxy for investigating overall magma output rate.

Starting around 11 Ma, the CGH range experienced three main periods of volcanic activity isolated by two long periods of relative quiescence (3.6–2.8 Ma and 1.5–0.9 Ma, Fig. 10A): first, a long and continuous period of activity between 10.6 to 3.6 Ma with a maximum pulse of activity at 6.6 Ma (contemporaneous to the growth of Seaca-Tătarca volcano); and next, a drastic decrease of volcanic activity with only episodic activities at 2.8–1.5 Ma and 1–0.03 Ma during the growth of Pilișca and Ciomadul. The migration of volcanism can be correlated to changes in the magma storage system (along with magma composition) influenced or triggered by changes in plate tectonic processes (see global context in Crisp, 1984; White et al., 2006; East Carpathian features in Mason et al., 1998; Seghedi et al., 2011). Before 3.6 Ma, most volcanoes (Fig. 10A, Fig. 10B and Fig. 10C) erupted relatively high volumes ($>50 \text{ km}^3$) of basaltic andesite to andesite lavas with a typical calc-alkaline composition (Seghedi et al., 2011). Their homogeneous Sr-Nd-Pb isotopic composition may

reflect a common mantle source (Mason et al., 1996, 1998; Seghedi et al., 2011). On the contrary, South Harghita volcanoes of the 3.6–0.03 Ma period (Fig. 10A and Fig. 10D) are smaller ($<30 \text{ km}^3$) and show different chemical composition with progressively increasing K-content (from calc-alkaline to high-K calc-alkaline and shoshonite) and adakite-like features, reflected by the increased proportions of dacites and shoshonites (Szakács et al., 1993; Seghedi et al., 2011).

The two different magma sources should have been responsible for the observed morphometric dichotomy in volcano size between the northern segments (from Călimani up to Luci-Lazu edifice in North Harghita) and the three last edifices (Cucu, Pilișca, Ciomadul in South Harghita). Such conclusions fit with observations of Crisp (1984) and White et al. (2006), who showed that more mafic magmas are more easily mobilized in the lithosphere and tend to erupt higher volumes (northern CGH volcanoes) than the differentiated ones (i.e. most of South Harghita).

Subsequent GR values computed at segment-scale (234, 276, 116 and $39 \text{ km}^3/\text{Ma}$ from north to south segments, Table 2) as well as values at volcano-scale ($>100 \text{ km}^3/\text{Ma}$ until 3.6 Ma and $<50 \text{ km}^3/\text{Ma}$ after) clearly support the decrease of volcanic intensity along the range, as previously identified by Szakács et al. (1995, 2018), and the effect of different magma sources (Seghedi et al., 2011). Moreover, Bouguer and magnetic anomalies surveys (Seghedi et al., 2019) revealed positive residual anomaly in the northern and axial part of the range, indicating the presence of high-density subvolcanic bodies which may be correlated to the high eruptive volumes computed in those segments. Contrarily, in the Southern Harghita, residual magnetic anomalies are negative, indicating the presence of low-density structures in coherence with the small volumes of volcanoes.

In Gurghiu segment, the main magmatic pulse of activity observed around 6.6 Ma (Fig. 10A) can be plausibly related to the migration of the subducted slab through the magma generating zone in the mantle and the initiation of the progressive detachment of the slab following an oblique subduction stage (Mason et al. 1998; Seghedi et al. 1998, 2011). This main pulse temporally coincides with an E–W compressional event that occurred across the entire Carpatho-Pannonian region during the late Miocene, interpreted as reflecting the arrival of thick and buoyant continental crust at the trench and its resistance to subduction (Peresson and Decker, 1997). Moreover, Gurghiu zone is mostly located at the intersection of regional tectonic elements with normal faults associated with paleo-basins (Seghedi et al., 2019). Interaction of tectonic structures would have created an area of low resistance, facilitating the penetration of magma and development of its ascent paths, thereby allowing rapid magma output and construction of large volcanic centres in this segment. Moreover, the largest positive magnetic anomaly identified under Gurghiu segment (Seghedi et al., 2019) was suggested to have been the solidified plumbing system responsible for generating the Seaca-Tătarca and Șumuleu volcanoes. Under a collisional regime, the progressive slab detachment toward the south (Fig. 10D) may have triggered gradual migration of magma production in South Harghita, along with emplacement of adjacent or overlapping volcanic structures (Mason et al., 1998; Seghedi et al., 2005b).

A decreasing volcano volume towards southeast (Szakács and Seghedi, 1995) (Fig. 4A; Table 2) can also be explained by the progressive opening of the lithospheric tear during slab steepening (Mason et al., 1998; Seghedi et al., 1998, 2011). Finally, during the final stages of subduction, a decrease in the convergence rate in the extreme south of the CGH (Fig. 10D) was evidenced (Seghedi et al., 2011), possibly also responsible for the smaller dimensions of the last three volcanoes.

The two Plio-Quaternary quiescence periods (3.6–2.8 and 1.5–0.9 Ma, Fig. 10A-D) were interpreted as linked to changes in magma sources by Seghedi et al. (2011). Interestingly, the 1.5–0.9 Ma time gap is a period when K-alkalic and Na-alkalic volcanism developed in other areas (shoshonites at Bixad/Malnaş and alkali-basalts in Perşani Mountains; Downes et al., 1995; Panaiotu et al., 2004).

Growth rate can be used as a good proxy for revealing the dynamism, fluctuation and intensity of volcanism. Globally, long-term eruption rates for silicic volcanism range from $<10^{-5}$ km³/ka to 10¹ km³/ka, the average being 2.3 ± 0.8 km³/ka for andesitic systems (Vidal and Bonneville, 2004; White et al., 2006). Plotting CGH growth rates results (Fig. 11) in the volcano volume versus lifespan graph of White et al. (2006) highlights two distinct magma output trends. The first group (most edifices of the three northernmost segments, plus Lucilazu volcano, blue symbols in Fig. 11) shows an average GR of 137 km³/Ma. The second one (the three youngest Pliocene-Quaternary edifices of South Harghita plus a small Late Miocene edifice in Gurghiu, red symbols in Fig. 11) is characterized by five times lower GR (28 km³/Ma).

Seaca-Tătarca volcano with the highest GR (825 km³/Ma, yellow symbol in Fig. 11) remains isolated from these two trends. The exceptionally high GR value does not only originate from the high precision on dating results, which allows drastically refining its lifespan (340 ka). Indeed, even considering the typical 1 Ma-long lifespan computed for most northern CGH volcanoes, its GR would remain two times higher than the given general trend. This implies both an exceptionally intense dynamism of Seaca-Tătarca activity and the call for getting more accurate age results for other volcanoes, since the lifespan of most CGH volcanoes probably could be in the same order of magnitude.

Over the entire CGH range, the calculated average GR is 200 km³/Ma (ratio between total volume emitted by all volcanoes during the whole range lifespan ~11Ma, without consideration of the repose periods), slightly larger than previously proposed 152-164 km³/Ma range (Szakács et al., 1997; Karátson and Timár, 2005). Even if fluctuations in CGH growth rate occurred through time (10-825 km³/Ma), values remain low compared to values for andesitic volcanoes (blue squares in Fig. 11 background) from other subduction-related arcs (White et al., 2006). It testifies to the less intense magma generation processes in the long term here than in areas where subduction is more intense, such as the West Indies, Japan and the Andes (White et al., 2006). Again, higher-precision dating may result in more intense GR at the lifetime scale of individual edifices as is the case with Seaca-Tătarca. Such a finding matches with worldwide (real, short-term) GR values of composite cones such as at Parinacota volcano, Chile (Hora et al., 2007).

6.5 Erosion rate and degree of denudation through time

Summing eroded volumes of all CGH volcanoes gives a total of 524±125 km³ (Table 2) and an average D_{Den} of 22%, close to the 23% proposed by Karátson and Timár (2005). At segment-scale, only the inferred eroded volume for Călimani segment (265±105 km³) does not match at 1 σ with the previous results of Karátson and Timár (2005), the new value being three times larger. The discrepancy, as presented above, rise from the difference in estimation of pre-erosional volumes (V_C) that directly impact on the estimation of eroded volumes.

At volcano-scale, the V_E vs V_C plot can be interpreted with respect to D_{Den} values as it is the ratio between these two parameters (Fig. Fig. 5B). Volcanoes with different volumes but experiencing the same D_{Den} rate (i.e. build at the more and less same period) would follow a linear correlation with constant slope (dashed lines in Fig. Fig. 5B). South Harghita volcanoes

built during Plio-Quaternary present the lowest D_{Den} values (~17%); average D_{Den} reaches 20% for 5.1-6.8 Ma old volcanoes and 27% for the older ones (>7.1 Ma; Călimani and northern volcanoes). On this graph, the vertical black arrows represent the additional of erosion affecting the older volcanoes and relatively to the average behaviour of the younger ones. This additional erosion increases with the volume of the volcano (bigger volcanoes produced more eroded material). However, in CGH range, larger volcanoes are also mostly the older ones, another parameter positively correlated to the V_E values (older volcanoes suffered longer erosion leading to larger eroded volume). Therefore, as volcano size (V_C) and age are globally positively correlated (Fig. 10A), these parameters sum these effects on V_E behaviour ($V_E = F(V_C) + G(Age)$). Nonetheless, even if the amount of erosion (V_E) seems to be nicely correlated to V_C , it is less relevant than the correlation between D_{Den} and the time (dashed line in Fig. 5B). By averaging D_{Den} values (Table 2 and black dots in Fig. 12) on each CGH segment leads to the following D_{Den} values: 30%, 25%, 20% and 15% (bottom of Table 2), confirming the progressive degradation of volcanoes toward north, as first quantified by (Karátson, 1996).

Correlation of the D_{Den} versus time allows establishing relationships between erosion rate (ER, i.e. aerial denudation or lowering of edifice height) and time. To better constrain the fast evolution of D_{Den} for the early stage of dismantling, we added to the CGH volcanoes dataset (this work, black dots in Fig. 12) the values proposed for the dozen edifices of the Ciomadul volcanic complex dating to between 0.03 and 0.8 Ma (Karátson et al., 2019; Lahitte et al., 2019, deduced D_{Den} summarised in supplementary material, grey dots in Fig. 12).

In the case of dismantling evolving through time according to a single behaviour, the trend of D_{Den} would evolve from 0 at $t=0$ (no erosion right after the volcano construction) to 100% after an infinite duration (with any volcano completely eroded). In order to verify D_{Den}

(0) = 0, the best function to fit such behaviour is a reverse exponential function ($D_{Den}(t)=1 - k.e^{-t}$), with $k=1$.

However, considering the exhaustive data set of denudation rate (0 to 11 Ma of denudation duration) leads to a best fit function with $k \sim 0.9$ that intersects the D_{Den} axis at 10% (dash blue line and y axis in Fig. 12). This means that a perfectly newly constructed volcano would have already lost 10% by dismantling right after its construction. This leads to an improvement of the D_{Den} behaviour, with the consideration of a more complex dismantling history, during the first 1 Ma of the erosion, when erosion occurred simultaneously to (and competed with) the growing volcano and just after the end of its construction. It is highlighted by the fast denudation rates affecting the domes of the Ciomadul complex (grey dots in Fig. 12), “instantaneously” erupted along the past 1 Ma. The good correlation between their age (i.e. erosion lifespan) and D_{Den} values supports interpretation of D_{Den} changes through time as better approximated by two distinct trends. First, a very fast evolving trend in the early stage with D_{Den} evolving from 0 to 14% during about the first 1 Ma (grey dots in Fig. 12). This trend also incorporates the proportion of the volcano dismantled during its 0.4-1 Ma-long construction phase (with an average proportion of 1% lost by 0.1 Ma-long lifespan). Then, a long-term (constrained by all other CGH volcanoes) trend fitted by the following equation (inset Fig. 12; see supplementary material for the detail of calculation):

$$D_{Den} = 1 - 0.89e^{-0.024t} \quad (R^2 = 0.62) \quad \text{with } t \text{ in Ma} \quad \text{Eq. 4}$$

Namely, the first stage of erosion (the first hundred thousand years [0 - <0.4 Ma] and, subsequently, with less intensity up to 0.8 Ma) is much more intense due to the presence of unafforested slopes, unconsolidated material (and possibly the erosion pattern inherited

from the activity period of the volcano) which result in high erosion rates. It is followed by a second slowly decelerating long-term trend that can be considered as steady-state erosion in the <20 Ma window.

Reciprocally, the averaged through time erosion rate (red and orange dots in Fig. 12) is fitted by a quickly decreasing function in the early stage, followed by a slowly decreasing rate (red curve in Fig. 12) with $R^2=0.72$. Both cumulated ER and D_{Den} parameters support a general behaviour that is time dependent.

In conclusion, our results fit with the already observed (Ruxton and McDougall, 1967; Francis, 1983; Karátson, 1996; Karátson et al., 2012) changes in volcano degradation: a short-term post-volcanic erosion (<0.8 Ma) was characterized by a rapid lowering and slope dissection/valley formation of the edifices with relatively high ER (24-39m/Ma, Fig. 12), followed by a drastic decrease until reaching an equilibrium stage, where erosion rate slowly decrease as mainly operating through a well-established drainage network (Ollier and Brown, 1971; Karátson, 1996; Karátson et al., 2012) (shown by the red curve based on orange and red dots in Fig. 12).

On the other hand, within the long-term erosion, there are obvious changes in ER values which can be linked to past climate variability. A crucial record for disentangling hydrographic evolution in the Black Sea–Carpathian area from Late Neogene has been provided by the marine core DSDP Site 380A (Leg 42B; Popescu, 2006). This record, along with the long-term trend in the palynological steppe index curve (Traverse, 1978) which is a proxy representative of past climate changes between cooler and warmer phases (Suc, 1984), indicates a continuously decreasing trend in warm and wet taxa for the Carpathian area throughout Late Neogene and a strong variability during the Quaternary (Popescu, 2002, 2006).

However, ER is expected to depend on several factors in addition to climate conditions such as lithology or edifice topography such as local slope (e.g. Cotton, 1952; Ollier and Brown, 1971; Francis, 1983; Karátson et al., 1999; Thouret, 1999; Reiners et al., 2003). Again, Fig. 6A clearly shows that morphometric parameters (e.g. height, area, volume) do not control denudation; therefore, erosion of CGH volcanoes is mostly controlled by hydroclimate variability and/or slope characteristics. For instance, Champagnac et al. (2014) showed, based on mountainous relief with 10-35° slope, that the behaviour followed by erosion over time can be approximated by a quadratic relationship. CGH volcanoes, with typically 10-21° slopes (Karátson, 2007), fit well with this observation. Therefore, since volcanoes in CGH present relatively uniform and moderate slopes and are largely dominated by andesite composite volcano types, we suggest that the contrasts in erosion have been mostly driven by past hydroclimate fluctuations with the relatively small impact of topography and rock strength.

From the integrated erosion rate (ER) at segment-scale (17, 11, 9, 28 m/Ma in Călimani, Gurghiu, North Harghita and South Harghita, respectively, Table 2), it is possible to infer the ER that the main specific time intervals the CGH range experienced (Karátson, 1996; Popescu, 2002, 2006; Erdei et al., 2007): 1) a short time period of subtropical-moderate continental transitional climate (Late Miocene, ~9.5-8.2 Ma); 2) a moderate continental climate with intervening semiarid periods (Late Miocene up to Pleistocene, ~8.2-4 Ma); and 3) a humid continental climate with periglacial regimes during the Pleistocene glaciations (Late Pliocene-Quaternary, from ~3.0 Ma up to present). Knowing the cumulated ER of the period t_1 and t_1+t_2 , we computed the specific ER driving dismantling during the period t_2 that leads to the cumulative ER of the period t_1+t_2 . For instance, the cumulated ER for North Harghita equals the erosion regime that specifically controlled the dismantling of North

Harghita before the construction of South Harghita plus the erosion regime during the dismantling of South Harghita. Obviously, the ER calculated for a certain period allows inferring the behaviour of erosion in response to prevailing climatic conditions.

This approach leads us to infer four successive erosion regimes showing a strong fluctuation over time (Table 3 and large diamonds in Fig. 12). 1) The highest ER (38 m/Ma, for the 10.8-6.9 Ma period, red diamond), obtained for the construction period of Călimani (Fig. 12), fits with the influence of the transitional moderate subtropical-continental climate period as defined above (Karátson, 1996; Popescu, 2002, 2006). 2) Decreasing ER for Gurghiu (14 m/Ma, 8.7-5.5 Ma, green diamond) and North Harghita (7 m/Ma, 7.0-4.6 Ma, blue diamond) accords with the subsequent, drastically decreased erosional processes characterizing a moderate continental climate. The extremely low value of 7 m/Ma, pointed out for Late Miocene to Pliocene times, can be explained by occasional semi-arid conditions (Lisiecki and Raymo, 2005). Indeed, Pliocene was already characterized by long-term shifts between the humid forest biotopes and run-off and the dry steppes, with changes linked to large amplitude climatic and moisture variations (Suc, 1984; Popescu, 2002, 2006). 4) Finally, the 28 m/Ma ER obtained for the Plio-Quaternary period (<3 Ma, yellow diamond) can reflect the prevailing more humid conditions (Suc, 1984; Karátson, 1996; Popescu, 2002, 2006); Schreiber and Unger, 2006) with a minor impact of glacial erosive activity and periglacial regime.

These results of erosion rate specific to the main time intervals analysed are following reconstructions of variability in sea levels and progressively stronger land glaciations from Late Neogene to recent times (Lisiecki and Raymo, 2005). These are correlated to a shift from prevalent chemical weathering during Late Neogene to enhanced surface processes, run-off and physical weathering prominent during the Quaternary (Gibbard and Lewin,

2009). The latter reflect rapid and high-amplitude successive hydroclimate variability between humid and glacial periods (colder and generally drier periglacial conditions) and shorter, wetter and warmer interglacials (Lisiecki and Raymo, 2005).

For the entire range, average ER is ~ 20 m/Ma, lower than the 31.5 m/Ma proposed by Karátson (1996). The latter value was calculated for the highest crater-topped summit regions only and consequently overestimated the average erosion rate over the whole area as omitting the peripheral aprons affected by lower ER. Our calculated ER for the highest volcanoes (Central Călimani, Fâncel-Lăpușna, Seaca-Tătarca, Vârghiș and Șumuleu) give high values (>14 m/Ma), whereas smallest edifices (Jirca, Bacta, Borzont, Râchitis, Pilișca) show the lowest values (<11 m/Ma, Table 3), in accordance with these ages, the most elevated (and larger in size) volcanoes are also the older ones.

Relying on inferences of past climatic variability for the broader Carpathian region and experienced by the CGH range throughout its evolution (Traverse, 1978; Suc, 1984; Karátson, 1996; Popescu, 2002, 2006; Erdei et al., 2007), we suggest that the best way to express ER variations is to detail them at the scale of an individual segment. Indeed, work at the scale of the whole CGH would only propose a regional value without consideration of variations through time, whereas work at the scale of a volcanic edifice would introduce local bias due to the own history of construction/dismantling that each volcano experienced (even if the 16 ERs define a general trend).

Globally, few studies have investigated ER over a long-term period, hence the relationship with the geodynamic context or past climate variability is still poorly understood (Karátson and Timár, 2005; Germa et al., 2010; Karátson et al., 2012a; Smith et al., 2016). Studies in tropical environments pointed out much higher ER (Louvât and Allègre, 1997; Hildenbrand et al., 2008; Germa et al., 2010; Ricci et al., 2015b). The systematically higher ER

values support the dominant role of climate as a main factor during dismantling. Moreover, differences in prevailing lithology can also affect the behaviour of ER. For example, basaltic rocks experience a faster weathering compared to andesitic ones and hence show higher ER (Gislason et al., 1996; Louvat and Allègre, 1997).

The termination of erosional processes on volcanic landforms is the complete destruction of the volcano with a remnant morphology of necks and dykes (i.e. skeleton stage: Cotton, 1952) and a D_{Den} reaching almost 100% (inset of Fig. 12). It defines a very long-term stage (tens to hundreds of Ma) when the volcano is very slowly dismantled as ER tend simultaneously to zero. The equation fitting D_{Den} long-term evolution (Eq. 4) leads to a duration required to destroy 95% of the entire range of 120 -20/+50 Ma. Even if such duration would be significantly modified by changes in the tectonic (e.g. uplift) and/or climatic contexts (Peulvast and Claudino Sales, 2005), its order of magnitude is reliable given some known relict morphologies that testify to Cretaceous or even older Mesozoic volcanism (Klein, 1975; Sturt et al., 1979; Simon-Coinçon, 1989; Slingerland and Furlong, 1989).

7 Conclusions

From the modelled volcanic surfaces performed in this study, the constrained constructed volumes allow classifying the CGH volcanoes in the field of volcanic massif, which is in accordance with their topographic complexities and eruptive lifespan, as pointed out by new ages of the Seaca-Tătarca (~340 ka) and Vârghiș (~900 ka) edifices. The 1/3-exponent in the power-law function relying original heights and volume advocates for CGH volcanoes as being self-similar, i.e. exhibiting homomorphic shapes irrespective of the peculiar complexities of their constructional histories. The overall volume computed for the

entire CGH is $\sim 2200 \text{ km}^3$, characterized by decreasing individual volumes from north to south, matches the evolution in terms of influence from different magma sources and plate tectonics. Individual growth rates per volcano distinguish a first moderate regime ($137 \text{ km}^3/\text{Ma}$) for the majority of volcanoes (11-3.6 Ma), followed by a drastically decreased output rate ($28 \text{ km}^3/\text{Ma}$) for the mostly Plio-Quaternary volcanoes. Apart from these two trends (representing the average of individual growth rate per volcano), the much higher GR obtained for Seaca-Tătarca ($825 \text{ km}^3/\text{Ma}$) is the consequence of probably both its shorter activity (inferred from new K-Ar datings) and a stronger magmatic regime. However, this finding also points out the poorly constrained duration of volcanic activity (and related output rates) if computed from poorly constrained ages in the case of CGH volcanoes for which modern standard dating is not yet available. Fluctuations of GR (relatively to the moderate overall averaged value of $200 \text{ km}^3/\text{Ma}$) is interpreted as the manifestation of strong fluctuations of volcanic activity driven by drastic changes in subduction mechanisms with decrease of convergence rate during the Plio-Quaternary causing breakoff beneath South Harghita and subsequent upwelling of asthenospheric mantle.

Beyond the average values of dismantling parameters (total eroded volume of $524 \pm 125 \text{ km}^3$, averaged denudation and erosion rate of 22% and 20 m/Ma , respectively), the correlation established between denudation and time defines two contrasting intensities of dismantling processes given their position along the erosional timeline. The first denudation trend shows an intense and rapid denudation ($< 0.8 \text{ Ma}$) after the cessation of volcanic activity while the second long-term trend slows down over the remaining erosional lifespan. Whereas this behaviour implies an almost constant erosion rate during the lifespan of the CGH erosion, detailed erosion rate values computed for shorter time intervals evidence the variety of intensity of erosion having occurred through time. Since volcanic edifices present

relatively uniform slopes and composition, these second order variations suggest that contrasts of ER along CGH range were mostly driven by climate fluctuations through time: highest ER (38 m/Ma) during the transitional moderate subtropical-continental climate period; intermediate ER (14 m/Ma) characterizing a moderate continental climate period when conditions became less humid; extremely low ER (7 m/Ma) coeval with continental, but occasionally semi-arid, climate; and, finally, higher ER (28 m/Ma) when Plio-Quaternary experienced generally wetter conditions with alternating glacial and interglacial stages.

The presented quantitative morphometric approach of paleo-volcanic landforms, performed at the detailed scale of individual volcanoes, demonstrates the possibility of a wide range of applications in various geological domains. They allow constraining constructive processes of volcano-tectonic dynamism at the scales of both individual volcanoes and global geodynamic context. Furthermore, by correlating eroded volumes and climatic variations, the intensity of the processes driving the dismantling of the volcanic range can also be well assessed.

Acknowledgments

We are particularly grateful to the two anonymous reviewers and Karoly Nemeth as well as Editor Markus Stoffel for their comments and suggestions, which greatly helped us to improve the clarity of this paper. This research has been supported by the Hungarian Scientific Research Fund NKFIH-OTKA No. 765 K 115472 to DK. Financial support for SD and PL was also provided by the SYSTER 2017 program 766 of INSU, CNRS. This is Laboratoire de Géochronologie Multi-Techniques (LGMT) contribution number 155.

833 **References**

- 834 Bablon, M., Quidelleur, X., Samaniego, P., Le Pennec, J.-L., Lahitte, P., Liorzou, C., Bustillos, J.E., Hidalgo, S., 2018. Eruptive
835 chronology of Tungurahua volcano (Ecuador) revisited based on new K-Ar ages and geomorphological reconstructions.
836 *Journal of Volcanology and Geothermal Research* 357, 378–398. <https://doi.org/10.1016/j.jvolgeores.2018.05.007>
- 837 Blaikie, T.N., van Otterloo, J., Ailleres, L., Betts, P.G., Cas, R.A.F., 2015. The erupted volumes of tephra from maar volcanoes
838 and estimates of their VEI magnitude: examples from the late Cenozoic Newer Volcanics Province, south-eastern Australia.
839 *Journal of Volcanology and Geothermal Research* 301, 81–89.
- 840 Borgia, A., 1994. Dynamic basis of volcanic spreading. *Journal of Geophysical Research: Solid Earth* 99, 17791–17804.
841 <https://doi.org/10.1029/94JB00578>
- 842 Borgia, A., Tizzani, P., Solaro, G., Manzo, M., Casu, F., Luongo, G., Pepe, A., Berardino, P., Fornaro, G., Sansosti, E., 2005.
843 Volcanic spreading of Vesuvius, a new paradigm for interpreting its volcanic activity. *Geophysical Research Letters* 32.
- 844 Champagnac, J.-D., Valla, P.G., Herman, F., 2014. Late-Cenozoic relief evolution under evolving climate: A review.
845 *Tectonophysics* 614, 44–65. <https://doi.org/10.1016/j.tecto.2013.11.037>
- 846 Ciupagea, D., Pauca, M., Ichim, T., 1970. *Geology of the Transylvanian depression*. Editura Academiei Republicii Socialiste
847 Romania, Bucharest.
- 848 Cotton, C.A., 1952. Volcanoes as landscape forms Whitcombe and Tombs. New Zealand.
- 849 Crisp, J.A., 1984. Rates of magma emplacement and volcanic output. *Journal of Volcanology and Geothermal Research* 20,
850 177–211. [https://doi.org/10.1016/0377-0273\(84\)90039-8](https://doi.org/10.1016/0377-0273(84)90039-8)
- 851 Csontos, L., Nagymarosy, A., Horváth, F., Kovac, M., 1992. Tertiary evolution of the Intra-Carpathian area: a model.
852 *Tectonophysics* 208, 221–241.
- 853 Delaney, P.T., 1992. You can pile it only so high. *Nature* 357, 194–196. <https://doi.org/10.1038/357194a0>
- 854 Demetrescu, C., Nielsen, S.B., Ene, M., Șerban, D.Z., Polonic, G., Andreescu, M., Pop, A., Balling, N., 2001. Lithosphere
855 thermal structure and evolution of the Transylvanian Depression—insights from new geothermal measurements and
856 modelling results. *Physics of the Earth and Planetary Interiors* 126, 249–267.

857 Downes, H., Seghedi, I., Szakács, A., Dobosi, G., James, D.E., Vaselli, O., Rigby, I.J., Ingram, G.A., Rex, D., Pécskay, Z., 1995.
858 Petrology and geochemistry of late Tertiary/Quaternary mafic alkaline volcanism in Romania. *Lithos* 35, 65–81.
859 [https://doi.org/10.1016/0024-4937\(95\)91152-Y](https://doi.org/10.1016/0024-4937(95)91152-Y)

860 Erdei, B., Hably, L., Kázmér, M., Utescher, T., Bruch, A.A., 2007. Neogene flora and vegetation development of the
861 Pannonian domain in relation to palaeoclimate and palaeogeography. *Palaeogeography, Palaeoclimatology, Palaeoecology*
862 253, 115–140.

863 Favalli, M., Fornaciai, A., 2017. Visualization and comparison of DEM-derived parameters. Application to volcanic areas.
864 *Geomorphology* 290, 69–84. <https://doi.org/10.1016/j.geomorph.2017.02.029>

865 Favalli, M., Innocenti, F., Pareschi, M.T., Pasquarè, G., Mazzarini, F., Branca, S., Cavarra, L., Tibaldi, A., 1999. The DEM of Mt.
866 Etna: geomorphological and structural implications. *Geodinamica Acta* 12, 279–290.

867 Favalli, M., Karátson, D., Mazzarini, F., Pareschi, M.T., Boschi, E., 2009. Morphometry of scoria cones located on a volcano
868 flank: A case study from Mt. Etna (Italy), based on high-resolution LiDAR data. *Journal of Volcanology and Geothermal*
869 *Research* 186, 320–330. <https://doi.org/10.1016/j.jvolgeores.2009.07.011>

870 Favalli, M., Karátson, D., Yepes, J., Nannipieri, L., 2014. Surface fitting in geomorphology — Examples for regular-shaped
871 volcanic landforms. *Geomorphology* 221, 139–149. <https://doi.org/10.1016/j.geomorph.2014.06.009>

872 Fielitz, W., Seghedi, I., 2005. Late Miocene–Quaternary volcanism, tectonics and drainage system evolution in the East
873 Carpathians, Romania. *Tectonophysics* 410, 111–136. <https://doi.org/10.1016/j.tecto.2004.10.018>

874 Francis, H., 1983. Magma and sediment—11 Problems of interpreting palaeovolcanics buried in the stratigraphic column 19.

875 Germa, A., Lahitte, P., Quidelleur, X., 2015. Construction and destruction of Mont Pelée volcano: Volumes and rates
876 constrained from a geomorphological model of evolution. *Journal of Geophysical Research: Earth Surface* 120, 1206–1226.
877 <https://doi.org/10.1002/2014JF003355>

878 Germa, A., Quidelleur, X., Labanieh, S., Chauvel, C., Lahitte, P., 2011. The volcanic evolution of Martinique Island: Insights
879 from K–Ar dating into the Lesser Antilles arc migration since the Oligocene. *Journal of Volcanology and Geothermal*
880 *Research* 208, 122–135. <https://doi.org/10.1016/j.jvolgeores.2011.09.007>

881 Germa, A., Quidelleur, X., Labanieh, S., Lahitte, P., Chauvel, C., 2010. The eruptive history of Morne Jacob volcano
882 (Martinique Island, French West Indies): Geochronology, geomorphology and geochemistry of the earliest volcanism in the
883 recent Lesser Antilles arc. *Journal of Volcanology and Geothermal Research* 198, 297–310.

884 Gibbard, P.L., Lewin, J., 2009. River incision and terrace formation in the Late Cenozoic of Europe. *Tectonophysics* 474, 41–
885 55.

886 Gislason, S.R., Arnorsson, S., Armannsson, H., 1996. Chemical weathering of basalt in Southwest Iceland; effects of runoff,
887 age of rocks and vegetative/glacial cover. *American Journal of Science* 296, 837–907.

888 Grosse, P., Euillades, P.A., Euillades, L.D., de Vries, B. van W., 2014. A global database of composite volcano morphometry.
889 *Bulletin of Volcanology* 76, 784.

890 Grosse, P., Kervyn, M., 2018. Morphometry of terrestrial shield volcanoes. *Geomorphology* 304, 1–14.
891 <https://doi.org/10.1016/j.geomorph.2017.12.017>

892 Grosse, P., Orihashi, Y., Guzman, S.R., Sumino, H., Nagao, K., 2018. Eruptive history of Incahuasi, Falso Azufre and El Condor
893 Quaternary composite volcanoes, southern Central Andes. *Bulletin of Volcanology* 80, 44. [https://doi.org/10.1007/s00445-](https://doi.org/10.1007/s00445-018-1221-5)
894 [018-1221-5](https://doi.org/10.1007/s00445-018-1221-5)

895 Grosse, P., van Wyk de Vries, B., Euillades, P.A., Kervyn, M., Petrinovic, I.A., 2012. Systematic morphometric
896 characterization of volcanic edifices using digital elevation models. *Geomorphology* 136, 114–131.
897 <https://doi.org/10.1016/j.geomorph.2011.06.001>

898 Grosse, P., van Wyk de Vries, B., Petrinovic, I.A., Euillades, P.A., Alvarado, G.E., 2009. Morphometry and evolution of arc
899 volcanoes. *Geology* 37, 651–654. <https://doi.org/10.1130/G25734A.1>

900 Hildenbrand, A., Gillot, P.-Y., Marlin, C., 2008. Geomorphological study of long-term erosion on a tropical volcanic ocean
901 island: Tahiti-Nui (French Polynesia). *Geomorphology* 93, 460–481. <https://doi.org/10.1016/j.geomorph.2007.03.012>

902 Hora, J.M., Singer, B.S., Wörner, G., 2007. Volcano evolution and eruptive flux on the thick crust of the Andean Central
903 Volcanic Zone: ⁴⁰Ar/³⁹Ar constraints from Volcán Parinacota, Chile. *Geological Society of America Bulletin* 119, 343–362.

904 Karátson, D., 2007. A Börzsönytől a Hargitáig—vulkanológia, felszínfejlődés, ősföldrajz. Typotex Kiadó, Budapest 463.

905 Karátson, D., 1996. Rates and factors of stratovolcano degradation in a continental climate: a complex morphometric
906 analysis for nineteen Neogene/Quaternary crater remnants in the Carpathians. *Journal of Volcanology and Geothermal*
907 *Research* 73, 65–78. [https://doi.org/10.1016/0377-0273\(96\)00016-9](https://doi.org/10.1016/0377-0273(96)00016-9)

908 Karátson, D., Favalli, M., Tarquini, S., Fornaciai, A., Wörner, G., 2010. The regular shape of stratovolcanoes: A DEM-based
909 morphometrical approach. *Journal of Volcanology and Geothermal Research* 193, 171–181.
910 <https://doi.org/10.1016/j.jvolgeores.2010.03.012>

911 Karátson, D., Telbisz, T., Dibacto, S., Lahitte, P., Szakács, A., Veres, D., Gertisser, R., Jánosi, Cs., Timár, G., 2019. Eruptive
912 history of the Late Quaternary Ciomadul (Csomád) volcano, East Carpathians, part II: magma output rates. *Bulletin of*
913 *Volcanology* 81. <https://doi.org/10.1007/s00445-019-1287-8>

914 Karátson, D., Telbisz, T., Harangi, S., Magyari, E., Dunkl, I., Kiss, B., Jánosi, C., Veres, D., Braun, M., Fodor, E., 2013.
915 Morphometrical and geochronological constraints on the youngest eruptive activity in East-Central Europe at the Ciomadul
916 (Csomád) lava dome complex, East Carpathians. *Journal of Volcanology and Geothermal Research* 255, 43–56.

917 Karátson, D., Telbisz, T., Woerner, G., 2012. Erosion rates and erosion patterns of Neogene to Quaternary stratovolcanoes
918 in the Western Cordillera of the Central Andes: An SRTM DEM based analysis. *Geomorphology* 139, 122–135.
919 <https://doi.org/10.1016/j.geomorph.2011.10.010>

920 Karátson, D., Thouret, J.-C., Moriya, I., Lomoschitz, A., 1999. Erosion calderas: origins, processes, structural and climatic
921 control. *Bulletin of Volcanology* 61, 174–193. <https://doi.org/10.1007/s004450050270>

922 Karátson, D., Timár, G., 2005. Comparative volumetric calculations of two segments of the Carpathian Neogene/Quaternary
923 volcanic chain using SRTM elevation data: implications for erosion and magma output rates, in: Thouret, J.C., Chester, D.K.
924 (Eds.), *Volcanic Landforms, Processes and Hazards*. pp. 19–35.

925 Karátson, D., Yepes, J., Favalli, M., Rodriguez-Peces, M.J., Fomaciai, A., 2016. Reconstructing eroded paleovolcanoes on
926 Gran Canaria, Canary Islands, using advanced geomorphometry. *Geomorphology* 253, 123–134.
927 <https://doi.org/10.1016/j.geomorph.2015.10.004>

928 Kereszturi, G., Németh, K., Cronin, S.J., Agustín-Flores, J., Smith, I.E., Lindsay, J., 2013. A model for calculating eruptive
929 volumes for monogenetic volcanoes—Implication for the Quaternary Auckland Volcanic Field, New Zealand. *Journal of*
930 *Volcanology and Geothermal Research* 266, 16–33.

931 Kervyn, M., Ernst, G.G.J., Carracedo, J.-C., Jacobs, P., 2012. Geomorphometric variability of “monogenetic” volcanic cones:
932 evidence from Mauna Kea, Lanzarote and experimental cones. *Geomorphology* 136, 59–75.

933 Klein, C., 1975. Massif armoricain et bassin parisien: contribution à l’étude géologique et géomorphologique d’un massif
934 ancien et de ses enveloppes sédimentaires: Normandie, Maine, Anjou, Touraine, Poitou septentrional et contrées
935 adjacentes. *Fondation Baulig*.

936 Krige, D.G., 1951. A statistical approach to some basic mine valuation problems on the Witwatersrand. *Journal of the*
937 *Southern African Institute of Mining and Metallurgy* 52, 119–139.

938 Lagabriele, Y., Guivel, C., Maury, R.C., Bourgois, J., Fourcade, S., Martin, H., 2000. Magmatic–tectonic effects of high
 939 thermal regime at the site of active ridge subduction: the Chile Triple Junction model. *Tectonophysics* 326, 255–268.

940 Lahitte, P., Dibacto, S., Karátson, D., Gertisser, R., Veres, D., 2019. Eruptive history of the Late Quaternary Ciomadul
 941 (Csomád) volcano, East Carpathians, part I: timing of lava dome activity. *Bulletin of Volcanology* 81.
 942 <https://doi.org/10.1007/s00445-019-1286-9>

943 Lahitte, P., Samper, A., Quidelleur, X., 2012. DEM-based reconstruction of southern Basse-Terre volcanoes (Guadeloupe
 944 archipelago, FWI): Contribution to the Lesser Antilles Arc construction rates and magma production. *Geomorphology* 136,
 945 148–164. <https://doi.org/10.1016/j.geomorph.2011.04.008>

946 Lang, B., Edelstein, O., Steinitz, G., Kovacs, M., Halga, S., 1994. Ar-Ar dating of adularia; a tool in understanding genetic
 947 relations between volcanism and mineralization; Baia Mare area (Gutii Mountains), northwestern Romania. *Economic*
 948 *Geology* 89, 174–180. <https://doi.org/10.2113/gsecongeo.89.1.174>

949 Lavigne, F., Degeai, J.-P., Komorowski, J.-C., Guillet, S., Robert, V., Lahitte, P., Oppenheimer, C., Stoffel, M., Vidal, C.M.,
 950 Surono, Pratomo, I., Wassmer, P., Hajdas, I., Hadmoko, D.S., de Belizal, E., 2013. Source of the great A.D. 1257 mystery
 951 eruption unveiled, Samalas volcano, Rinjani Volcanic Complex, Indonesia. *Proc Natl Acad Sci USA* 110, 16742.
 952 <https://doi.org/10.1073/pnas.1307520110>

953 Le Friant, A., Harford, C.L., Deplus, C., Boudon, G., Sparks, R.S.J., Herd, R.A., Komorowski, J.C., 2004. Geomorphological
 954 evolution of Montserrat (West Indies): importance of flank collapse and erosional processes. *Journal of the Geological*
 955 *Society* 161, 147–160. <https://doi.org/10.1144/0016-764903-017>

956 Leverington, D.W., Teller, J.T., Mann, J.D., 2002. A GIS method for reconstruction of late Quaternary landscapes from
 957 isobase data and modern topography. *Computers & Geosciences* 28, 631–639.

958 Lisiecki, L.E., Raymo, M.E., 2005. A Pliocene-Pleistocene stack of 57 globally distributed benthic $\delta^{18}\text{O}$ records.
 959 *Paleoceanography* 20.

960 Lexa, J., Seghedi, I., Nemeth, K., Szakács, A., Konecny, V., Pécskay, Z., Fuegoep, A., Kovacs, M., 2010. Neogene-Quaternary
 961 Volcanic forms in the Carpathian-Pannonian Region: a review. *Central European Journal of Geosciences* 2, 207-U75.
 962 <https://doi.org/10.2478/v10085-010-0024-5>

963 Louvat, P., Allègre, C.J., 1997. Present denudation rates on the island of Réunion determined by river geochemistry: Basalt
 964 weathering and mass budget between chemical and mechanical erosions. *Geochimica et Cosmochimica Acta* 61, 3645–
 965 3669. [https://doi.org/10.1016/S0016-7037\(97\)00180-4](https://doi.org/10.1016/S0016-7037(97)00180-4)

966 Magyari, E.K., Veres, D., Wennrich, V., Wagner, B., Braun, M., Jakab, G., Karatson, D., Pal, Z., Ferenczy, G., St-Onge, G.,
 967 Rethemeyer, J., Francois, J.-P., von Reumont, F., Schaebitz, F., 2014. Vegetation and environmental responses to climate
 968 forcing during the Last Glacial Maximum and deglaciation in the East Carpathians: attenuated response to maximum cooling
 969 and increased biomass burning. *Quaternary Science Reviews* 106, 278–298.
 970 <https://doi.org/10.1016/j.quascirev.2014.09.015>

971 Mason, P.R.D., Downes, H., Thirlwall, M.F., Seghedi, I., Szakács, A., Lowry, D., Matthey, D., 1996. Crustal Assimilation as a
 972 Major Petrogenetic Process in the East Carpathian Neogene and Quaternary Continental Margin Arc, Romania. *Journal of*
 973 *Petrology* 37, 927–959. <https://doi.org/10.1093/petrology/37.4.927>

974 Mason, P.R.D., Seghedi, I., Szákacs, A., Downes, H., 1998. Magmatic constraints on geodynamic models of subduction in the
 975 East Carpathians, Romania. *Tectonophysics* 297, 157–176. [https://doi.org/10.1016/S0040-1951\(98\)00167-X](https://doi.org/10.1016/S0040-1951(98)00167-X)

976 Matenco, L., Bertotti, G., 2000. Tertiary tectonic evolution of the external East Carpathians (Romania). *Tectonophysics* 316,
 977 255–286.

978 Matenco, L., Krézsek, C., Merten, S., Schmid, S., Cloetingh, S., Andriessen, P., 2010. Characteristics of collisional orogens
 979 with low topographic build-up: an example from the Carpathians. *Terra Nova* 22, 155–165. [https://doi.org/10.1111/j.1365-](https://doi.org/10.1111/j.1365-3121.2010.00931.x)
 980 [3121.2010.00931.x](https://doi.org/10.1111/j.1365-3121.2010.00931.x)

981 Merle, O., Borgia, A., 1996. Scaled experiments of volcanic spreading. *Journal of Geophysical Research: Solid Earth* 101,
 982 13805–13817. <https://doi.org/10.1029/95JB03736>

983 Molnár, K., Harangi, S., Lukács, R., Dunkl, I., Schmitt, A.K., Kiss, B., Garamhegyi, T., Seghedi, I., 2018. The onset of the
 984 volcanism in the Ciomadul Volcanic Dome Complex (Eastern Carpathians): Eruption chronology and magma type variation.
 985 *Journal of Volcanology and Geothermal Research* 354, 39–56. <https://doi.org/10.1016/j.jvolgeores.2018.01.025>

986 Németh, K., Palmer, J., 2019. Geological mapping of volcanic terrains: Discussion on concepts, facies models, scales, and
 987 resolutions from New Zealand perspective. *Journal of Volcanology and Geothermal Research* 385, 27–45.

988 Ollier, C.D., Brown, M.J.F., 1971. Erosion of a young volcano in New Guiana. *Zeitschrift fur Geomorphologie* 15, 12–28.

989 Panaiotu, C.G., Pécskay, Z., Hambach, U., Seghedi, I., Panaiotu, C.E., Tetsumaru, I., Orleanu, M., Szakács, A., 2004. Short-
 990 lived quaternary volcanism in the Persani Mountains (Romania) revealed by combined K-Ar and paleomagnetic data.
 991 *Geologica Carpathica* 55, 333–339.

992 Pécskay, Edelstein, O., Seghedi, I., Szakács, A., Marinel, K., Crihan, I.-M., Bernad, A., 1995. K-Ar datings of Neogene-
993 Quaternary calc-alkaline volcanic rocks in Romania.

994 Pécskay, Z., Lexa, J., Szakács, A., Seghedi, I., Balogh, K., Konecny, V., Zelenka, T., Kovacs, M., Poka, T., Fulop, A., Marton, E.,
995 Panaiotu, C., Cvetkovic, V., 2006. Geochronology of Neogene magmatism in the Carpathian arc and intra-Carpathian area.
996 *Geologica Carpathica* 57, 511–530.

997 Peltz, S., Vajdea, E., Balogh, K., Pécskay, Z., 1987. Contributions to the chronological study of the volcanic processes in the
998 Călimani and Harghita Mountains (East Carpathians, Romania). *Compte Rendu de Institute de Geologie e Geofisique* 72, 1.

999 Peresson, H., Decker, K., 1997. Far-field effects of Late Miocene subduction in the Eastern Carpathians: E-W compression
1000 and inversion of structures in the Alpine-Carpathian-Pannonian region. *Tectonics* 16, 38–56.
1001 <https://doi.org/10.1029/96TC02730>

1002 Persson, K.S., Garcia-Castellanos, D., Sokoutis, D., 2004. River transport effects on compressional belts: First results from an
1003 integrated analogue-numerical model. *Journal of Geophysical Research: Solid Earth* 109.

1004 Peulvast, J.-P., Claudino Sales, V., 2005. Surfaces d'aplanissement et géodynamique. *Géomorphologie : relief, processus,*
1005 *environnement* 11, 249–274. <https://doi.org/10.4000/geomorphologie.605>

1006 Popescu, S.-M., 2006. Late Miocene and early Pliocene environments in the southwestern Black Sea region from high-
1007 resolution palynology of DSDP Site 380A (Leg 42B). *Palaeogeography, Palaeoclimatology, Palaeoecology* 238, 64–77.

1008 Popescu, S.-M., 2002. Repetitive changes in Early Pliocene vegetation revealed by high-resolution pollen analysis: revised
1009 cyclostratigraphy of southwestern Romania. *Review of Palaeobotany and Palynology* 120, 181–202.

1010 Rădulescu, D.P., Săndulescu, M., 1973. The plate-tectonics concept and the geological structure of the Carpathians.
1011 *Tectonophysics* 16, 155–161. [https://doi.org/10.1016/0040-1951\(73\)90010-3](https://doi.org/10.1016/0040-1951(73)90010-3)

1012 Reiners, P.W., Ehlers, T.A., Mitchell, S.G., Montgomery, D.R., 2003. Coupled spatial variations in precipitation and long-term
1013 erosion rates across the Washington Cascades. *Nature* 426, 645–647. <https://doi.org/10.1038/nature02111>

1014 Ricci, J., Lahitte, P., Quidelleur, X., 2015a. Construction and destruction rates of volcanoes within tropical environment:
1015 Examples from the Basse-Terre Island (Guadeloupe, Lesser Antilles). *Geomorphology* 228, 597–607.
1016 <https://doi.org/10.1016/j.geomorph.2014.10.002>

1017 Ricci, J., Quidelleur, X., Lahitte, P., 2015b. Volcanic evolution of central Basse-Terre Island revisited on the basis of new
1018 geochronology and geomorphology data. *Bulletin of Volcanology* 77, 84.

1019 Ruxton, B.P., McDougall, I., 1967. Denudation rates in northeast Papua from potassium-argon dating of lavas. *American*
1020 *Journal of Science* 265, 545–561.

1021 Salvany, T., Lahitte, P., Nativel, P., Gillot, P.-Y., 2012. Geomorphic evolution of the Piton des Neiges volcano (Réunion Island,
1022 Indian Ocean): Competition between volcanic construction and erosion since 1.4Ma. *Geomorphology* 136, 132–147.
1023 <https://doi.org/10.1016/j.geomorph.2011.06.009>

1024 Samper, A., Quidelleur, X., Lahitte, P., Mollex, D., 2007. Timing of effusive volcanism and collapse events within an oceanic
1025 arc island: Basse-Terre, Guadeloupe archipelago (Lesser Antilles Arc). *Earth and Planetary Science Letters* 258, 175–191.
1026 <https://doi.org/10.1016/j.epsl.2007.03.030>

1027 Sandulescu, M., 1988. Cenozoic Tectonic History of the Carpathians: Chapter 2.

1028 Schreiber, W., Unger, E., 2006. Some specific aspects of postvolcanic relief evolution in the Harghita Mountains. (in
1029 Hungarian with English abstract). *Földtani Közlöny*, 136/1, 285–298.

1030 Seghedi, Downes, H., Harangi, S., Mason, P.R.D., Pécskay, Z., 2005a. Geochemical response of magmas to Neogene-
1031 Quaternary continental collision in the Carpathian-Pannonian region: A review. *Tectonophysics* 410, 485–499.
1032 <https://doi.org/10.1016/j.tecto.2004.09.015>

1033 Seghedi, I., 1995. The Călimani-Gurghiu-Harghita volcanic chain, East Carpathians, Romania: volcanological features.

1034 Seghedi, I., Balintoni, I., Szakács, A., 1998. Interplay of tectonics and neogene post-collisional magmatism in the
1035 intracarpathian region. *Lithos* 45, 483–497. [https://doi.org/10.1016/S0024-4937\(98\)00046-2](https://doi.org/10.1016/S0024-4937(98)00046-2)

1036 Seghedi, I., Downes, H., Vaselli, O., Szakács, A., Balogh, K., Pécskay, Z., 2004a. Post-collisional Tertiary–Quaternary mafic
1037 alkalic magmatism in the Carpathian–Pannonian region: a review. *Tectonophysics* 393, 43–62.
1038 <https://doi.org/10.1016/j.tecto.2004.07.051>

1039 Seghedi, I., Mațenco, L., Downes, H., Mason, P.R.D., Szakács, A., Pécskay, Z., 2011. Tectonic significance of changes in post-
1040 subduction Pliocene–Quaternary magmatism in the south east part of the Carpathian–Pannonian Region. *Tectonophysics*
1041 502, 146–157. <https://doi.org/10.1016/j.tecto.2009.12.003>

1042 Seghedi, I., Mirea, V., Popa, R.-G., Szakács, A., 2019. Tectono-magmatic characteristics of post-collisional magmatism: Case
1043 study East Carpathians, Călimani-Gurghiu-Harghita volcanic range. *Physics of the Earth and Planetary Interiors* 293, 106270.
1044 <https://doi.org/10.1016/j.pepi.2019.106270>

- 1045 Seghedi, I., Szakács, A., Snelling, N.J., Pécskay, Z., 2004b. Evolution of the Neogene Gurghiu Mountains volcanic range
1046 (Eastern Carpathians, Romania), based on K-Ar geochronology. *Geologica Carpathica* 55, 325–332.
- 1047 Seghedi, Szakács, A., Pécskay, Z., Mason, P.R.D., 2005b. Eruptive history and age of magmatic processes in the Călimani
1048 volcanic structure (Romania) 10.
- 1049 Simon-Coinçon, R., 1989. Le rôle des paléooltérations et des paléofomes dans les socles : l'exemple du Rouergue (Massif
1050 Central français). Centre de géologie générale et minière.
- 1051 Slingerland, R., Furlong, K.P., 1989. Geodynamic and geomorphic evolution of the Permo-Triassic Appalachian Mountains.
1052 *Geomorphology* 2, 23–37.
- 1053 Smith, S.G., Wegmann, K.W., Ancuta, L.D., Gosse, J.C., Hopkins, C.E., 2016. Paleotopography and erosion rates in the central
1054 Hangay Dome, Mongolia: Landscape evolution since the mid-Miocene. *Journal of Asian Earth Sciences* 125, 37–57.
1055 <https://doi.org/10.1016/j.jseaes.2016.05.013>
- 1056 Sturt, B.A., Dalland, A., Mitchell, J.L., 1979. The age of the sub Mid-Jurassic tropical weathering profile of Andoya, northern
1057 Norway, and the implications for the late Palaeozoic palaeography in the North Atlantic region. *Geologische Rundschau* 68,
1058 523–542.
- 1059 Suc, J.-P., 1984. Origin and evolution of the Mediterranean vegetation and climate in Europe. *Nature* 307, 429.
- 1060 Szabó, C., Harangi, S., Csontos, L., 1992. Review of Neogene and Quaternary volcanism of the Carpathian-Pannonian region
1061 14.
- 1062 Szakács, A., Ioane, D., Seghedi, I., Rogobete, M., Pécskay, Z., 1997. Rates of migration of volcanic activity and magma out
1063 put along the Calimani-Gurghiu-Harghita volcanic range, East Carpathians, Romania. *Przegląd Geologiczny* 45, 1106.
- 1064 Szakács, A., Krézsek, C., 2006. Volcano–basement interaction in the Eastern Carpathians: Explaining unusual tectonic
1065 features in the Eastern Transylvanian Basin, Romania. *Journal of Volcanology and Geothermal Research* 158, 6–20.
1066 <https://doi.org/10.1016/j.jvolgeores.2006.04.012>
- 1067 Szakács, A., Seghedi, I., 2000. Large volume volcanic debris avalanche in the East Carpathians, Romania. *Volcaniclastic rocks,*
1068 *from magmas to sediments*, Gordon Breach Science Publishers, Amsterdam, The Netherlands 131–151.
- 1069 Szakács, A., Seghedi, I., 1996. Volcaniclastic sequences around andesitic stratovolcanoes, East Carpathians, Romania.
1070 *Romanian Journal of Petrology* 77, 1–55.

- 1071 Szakács, A., Seghedi, I., 1995. The Călimani-Gurghiu-Harghita volcanic chain. East Carpathians.
- 1072 Szakács, A., Seghedi, I., Pécskay, Z., 1993. Peculiarities of South Harghita Mts as a Terminal Segment of the Carpathian
1073 Neogene to Quaternary Volcanic Chain. Editura Academiei Române.
- 1074 Székely, B., Karátson, D., 2004. DEM-based morphometry as a tool for reconstructing primary volcanic landforms: examples
1075 from the Börzsöny Mountains, Hungary. *Geomorphology* 63, 25–37. <https://doi.org/10.1016/j.geomorph.2004.03.008>
- 1076 Tari, G., Dövényi, P., Dunkl, I., Horváth, F., Lenkey, L., Stefanescu, M., Szafián, P., Tóth, T., 1999. Lithospheric structure of the
1077 Pannonian basin derived from seismic, gravity and geothermal data. Geological Society, London, Special Publications 156,
1078 215–250.
- 1079 Thouret, J.-C., 1999. Volcanic geomorphology—an overview. *Earth-Science Reviews* 47, 95–131.
1080 [https://doi.org/10.1016/S0012-8252\(99\)00014-8](https://doi.org/10.1016/S0012-8252(99)00014-8)
- 1081 Thouret, J.-C., Oehler, J.-F., Gupta, A., Solikhin, A., Procter, J.N., 2014. Erosion and aggradation on persistently active
1082 volcanoes—a case study from Semeru Volcano, Indonesia. *Bulletin of Volcanology* 76, 857.
- 1083 Traverse, A., 1978. Palynological analysis of DSDP Leg 42B (1975) cores from the Black Sea. Initial Report DSDP 42, 993–
1084 1016.
- 1085 Tucker, G.E., Hancock, G.R., 2010. Modelling landscape evolution. *Earth Surface Processes and Landforms* 35, 28–50.
- 1086 Vidal, V., Bonneville, A., 2004. Variations of the Hawaiian hot spot activity revealed by variations in the magma production
1087 rate. <https://doi.org/10.1029/2003JB002559>
- 1088 Wadge, G., 1984. Comparison of volcanic production rates and subduction rates in the Lesser Antilles and Central America.
1089 *Geology* 12, 555–558.
- 1090 Wadge, G., 1982. Steady state volcanism: Evidence from eruption histories of polygenetic volcanoes. *Journal of Geophysical*
1091 *Research: Solid Earth* 87, 4035–4049. <https://doi.org/10.1029/JB087iB05p04035>
- 1092 White, S.M., Crisp, J.A., Spera, F.J., 2006. Long-term volumetric eruption rates and magma budgets. *Geochemistry,*
1093 *Geophysics, Geosystems* 7. <https://doi.org/10.1029/2005GC001002>
- 1094 Wooller, L., van Wyk de Vries, B., Murray, J.B., Rymer, H., Meyer, S., 2004. Volcano spreading controlled by dipping
1095 substrata. *Geology* 32, 573. <https://doi.org/10.1130/G20472.1>

- 1096 Wright, R., Garbeil, H., Baloga, S.M., Mouginis-Mark, P.J., 2006. An assessment of shuttle radar topography mission digital
1097 elevation data for studies of volcano morphology. *Remote Sensing of Environment* 105, 41–53.
- 1098 Yokoyama, R., Shirasawa, M., Pike, R.J., 2002. Visualizing Topography by Openness: A New Application of Image Processing
1099 to Digital Elevation Models.
- 1100 Zernack, A.V., Cronin, S.J., Neall, V.E., Procter, J.N., 2011. A medial to distal volcanoclastic record of an andesite
1101 stratovolcano: detailed stratigraphy of the ring-plain succession of south-west Taranaki, New Zealand. *International Journal*
1102 *of Earth Sciences* 100, 1937–1966.

Figure Captions

Fig. 1: Geological setting of the studied area (East Carpathian Volcanic Range). Each volcano is labelled as following (Romanian names, Hungarian ones can be found in Table 1): Călimani sector (surrounded by red outline): 01 – Central Călimani including Rusca-Tihu cones Lucaciul, Tămăul and Călimani caldera; 02 – Moldovanul. Gurghiu sector (green outline): 03 – Jirca; 04 – Fâncel-Lăpuşna, including cones Fâncel (04a) and Obarsia (04b); 05 – Bacta; 06 – Seaca-Tătarca; 07 – Ciumani; 08 – Borzont; 09 – Şumuleu including cone Şumuleu (09a) and Vf. Ascuţit (09b). North Harghita sector (blue outline): 10 – Ostoros; 11 – Ivo-Cocoizaş; 12 – Râchitis; 13a – Vârghiş and 13b – Szeles Vésze cone. South Harghita sector (yellow outline): 14 – Luci-Lazu (14a and 14b); 15 – Cucu; 16 – Pilişca; 17 – Ciomadul lavas domes. Inset: Regional topographic sketch map of Carpathian orogen.

Fig. 2 : A) Constraining points (CPs) of each single volcanic edifice. New unspiked K/Ar ages (in Ma): A) Călimani. B) Seaca-Tătarca volcano. C) Vârghiş volcano. D) Pilişca volcano.

Fig. 3 : Modelling of the best fitting surface with all relevant parameters, example of Seaca-Tătarca volcano: A) Elevation versus distance to centre diagram, green dots project the whole volcano surface, purple dots are CPs and black dots are the best model profile. B) Projection of mean (orange), max (yellow) and min (grey) elevation of the whole volcano surface, after a summarization by a 100m-long window. Note how the best model profile (black dot) fit well with the upper surface (yellow dots). Average altitude loss (blue dots) computed as the difference between the best model profile and the mean elevation profile. C) Perspective view of the best modelled surface: purple dots are the CPs extracted from the

DEM (coloured surface). Coloured dots show the best modelled surface. Black sticks highlight the loss of elevation (i.e. the intensity of erosion).

Fig. 4 : Modelled paleo-volcanic surfaces (as they would be directly after the cessation of volcanism, i.e. before erosion effect): A) North (red colours) - South (yellow colours) cross-section and perspective views of the whole reconstructed CGH range. B), C), D) zoomed representation of Gurghiu, North Harghita and South Harghita sectors, respectively. Numbers refer as the same labels as in Fig. 1 and Table 2. Cream coloured surface is the pre-volcanic basement surface (PVBS).

Fig. 5 : A) Correlation between total constructed volume with volcano area (uncertainties displayed at 1σ -level): Green line and box parameters: power-law fitting function obtained with consideration of all volcanoes. Black line and box parameters: fitting without consideration of Făncel-Lăpușna volcano (green dot). Inset: height and volume of CGH volcanoes plotted on the height versus volume diagram of Grosse et al. (2009) with fitting power-law function. **B)** Correlation of eroded volume with constructed volume of each CGH volcano: circle diameters with respect to degree of denudation values (expressed in %). Colour of symbols, line and parameters box refer to volcano ages: older (red), intermediate (green) and youngest (yellow) volcanoes. Black line and parameters box represent the V_E - V_C correlations for all volcanoes whereas colour lines show fitting for the corresponding periods. Black arrow explained in text.

Fig. 6 : Correlation between degree of denudation of each volcano of the range with **A)** the height. **B)** the latitude. Colours symbols with respect to belonging segment (yellow: South Harghita, blue: North Harghita, green: Gurghiu, red; Călimani).

Fig. 7 : Relative uncertainty of constructed volume versus average height diagram with best fitting function. Circle diameter proportional to volcano volume.

Fig. 8 : Model of growth of Seaca-Tătarca volcano through time: **A)** Projection in elevation versus distance to centre of the whole Seaca-Tătarca volcano surface (green dots) with projection of the dated samples (white dots). Blue line displays the chronological model of growth based on the modelled uppermost volcanic surface. Note how the blue lines regularly spaced every each 10% of volume become closer upward. **B)** Proportions of constructed of Seaca-Tătarca volcano versus time diagram. White dots: growth proportion associated to each dated sample deduced from Fig. 8A, red dots represent interpolation of 0 and 100% of construction (i.e. begin and end of the activity).

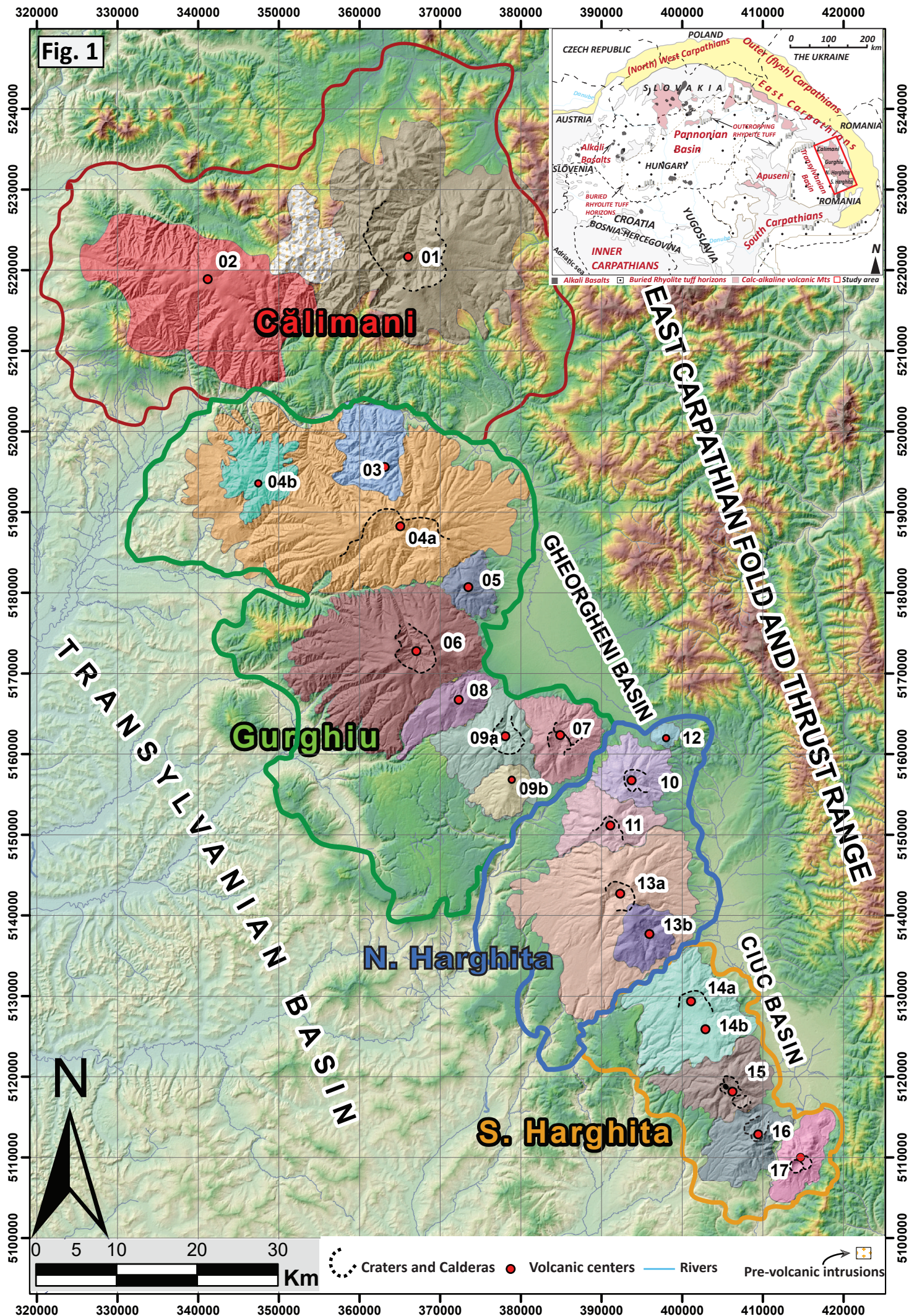
Fig. 9 : All available ages of CGH volcanic range projected along a N-S profile (Y-axis is the UTM coordinates of samples). Colours symbols as in Fig. 5 except grey symbols plotting newly dated samples. Coloured outlines display the spatio-temporal range of volcanic activity. Heavy lines show either the expansion (Gurghiu case, using only heavily outlined green symbols) or migration (N. and S. Harghita cases, using all their respective ages) through time (details in the text), with quantification in the coloured rectangles. Black double arrows highlight the synchronism in sectors.

Fig. 10 : Cumulative volume and magma output rates through time (A), correlated to the main Tertiary tectonic events affecting the East Carpathian range (displayed as cartoons B, C and D). **A)** Individual variation of volcanic output through time (coloured lines). Cumulative erupted volume (dashed line and left axis) and global growth rate (plain line and right axis) variations through time over the whole CGH range. Inset displays Fig. 10 to highlight volume – space correlations. **B)** Oceanic crust subduction occurring during the Early–Mid-Miocene

convergence episode. **C)** Thinned continental crust subduction and collisional features in the overriding plate. **D)** Slab detachment of the dense oceanic lithosphere from buoyant continental lithosphere and upwelling of the hot asthenospheric mantle into the gap to be juxtaposed against the base of the mechanical lithosphere.

Fig. 11 : Volumes versus lifespan in a log-log diagram. Trends of both group (red and blue diagonal lines) as well as grey dashed lines represent constant rates of magma output. Background of the figure displaying various volcanic contexts around the world from White et al. (2006).

Fig. 12 : Graph of dismantling parameters versus time. Black and grey circles (left axis) are the computed degree of denudation values of each volcano (i.e. averaged along its whole erosion history), fitted by the reverse exponential curve (with parameters in the blue box). Grey circles are values from the dozen domes of the Ciomadul volcanic complex (Karátson et al., 2019; Lahitte et al., 2019; details in S.M.), black dots are D_{Den} values from this work (all other CGH volcanoes). Orange and red circles are the cumulative averaged erosion rate of each volcano (right axis) and fitted by the red quadratic curve. Contrarily to red/orange circles that show average-integrated erosion rates, large diamonds (right axis) represent the erosion rates computed for specific periods when specific climatic context (summarized on top of the figure) occurred: red diamond for erosion regime occurring during 10.8 - 6.9 Ma; green diamond: 8.7 - 5.5 Ma; blue diamond: 7.0-4.6 Ma; yellow diamond: Quaternary.



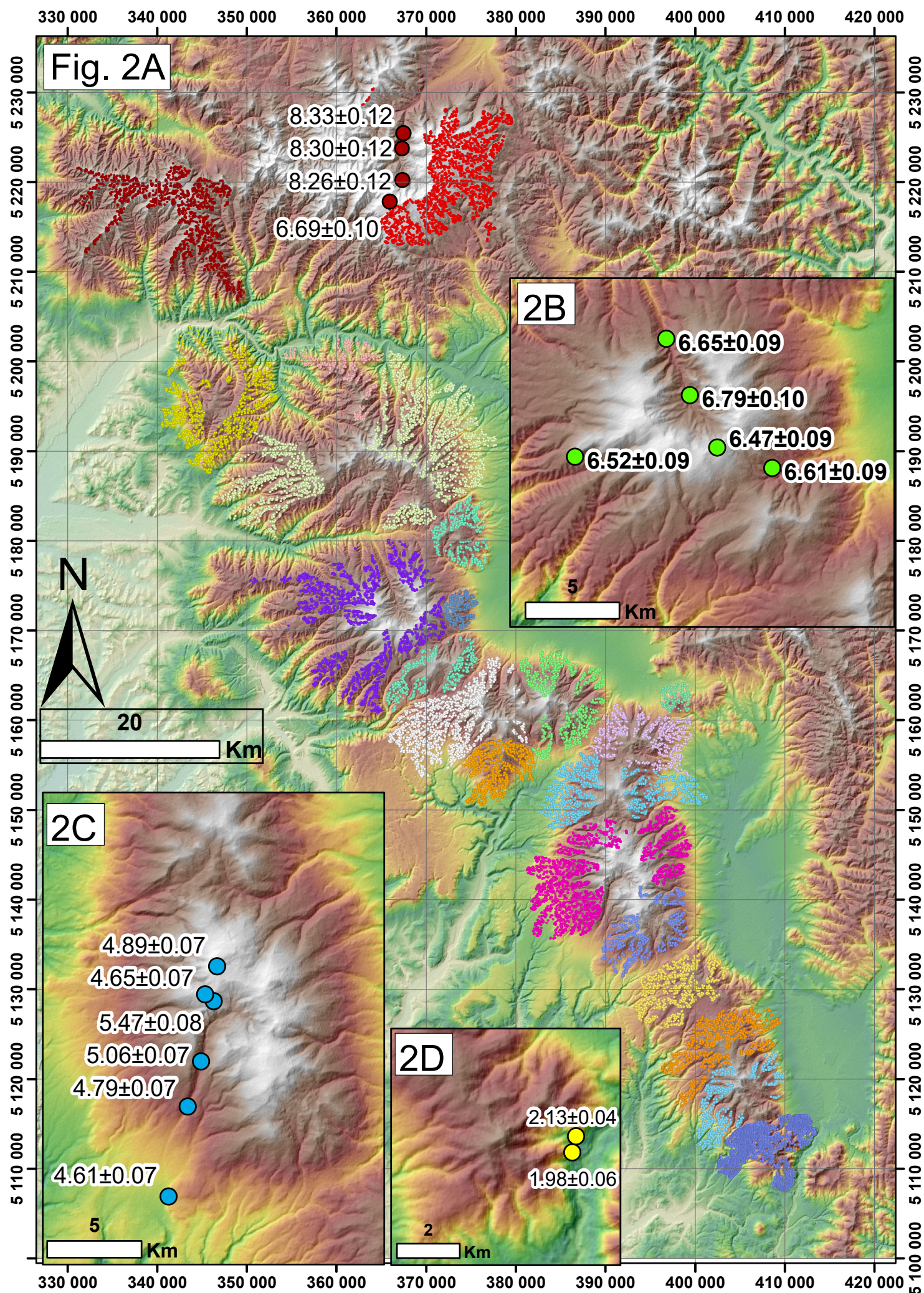


Fig. 3

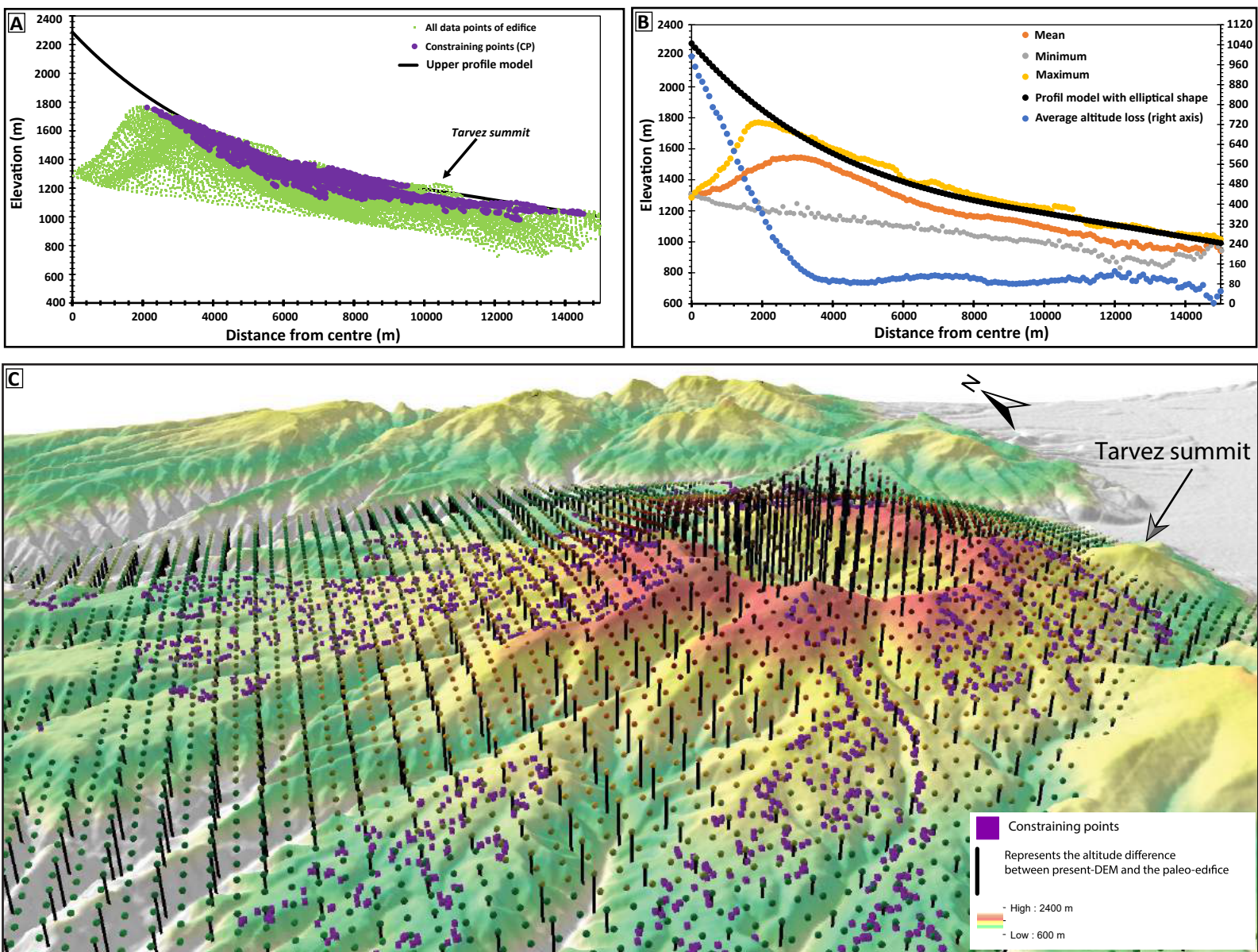


Fig. 4

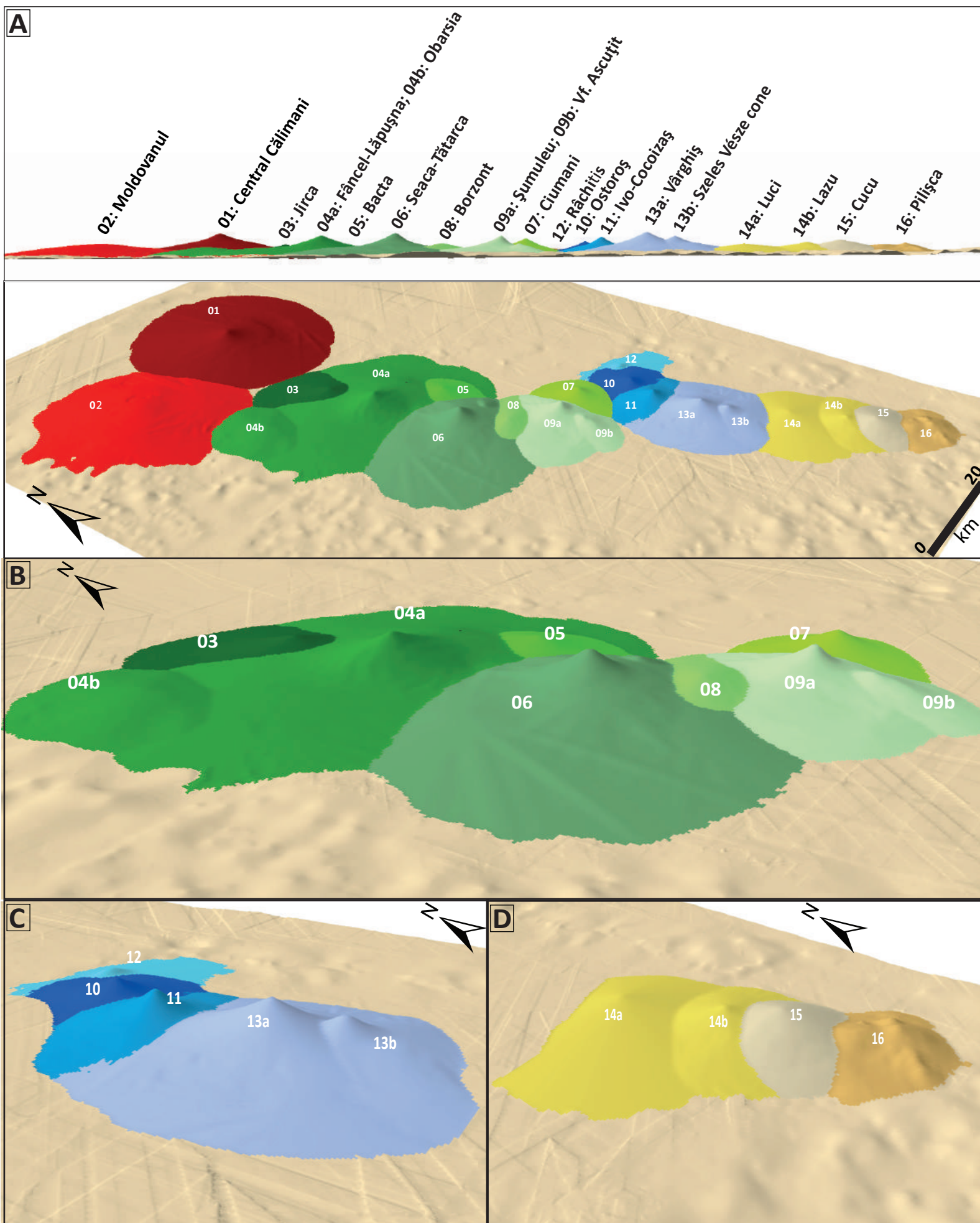


Fig. 5

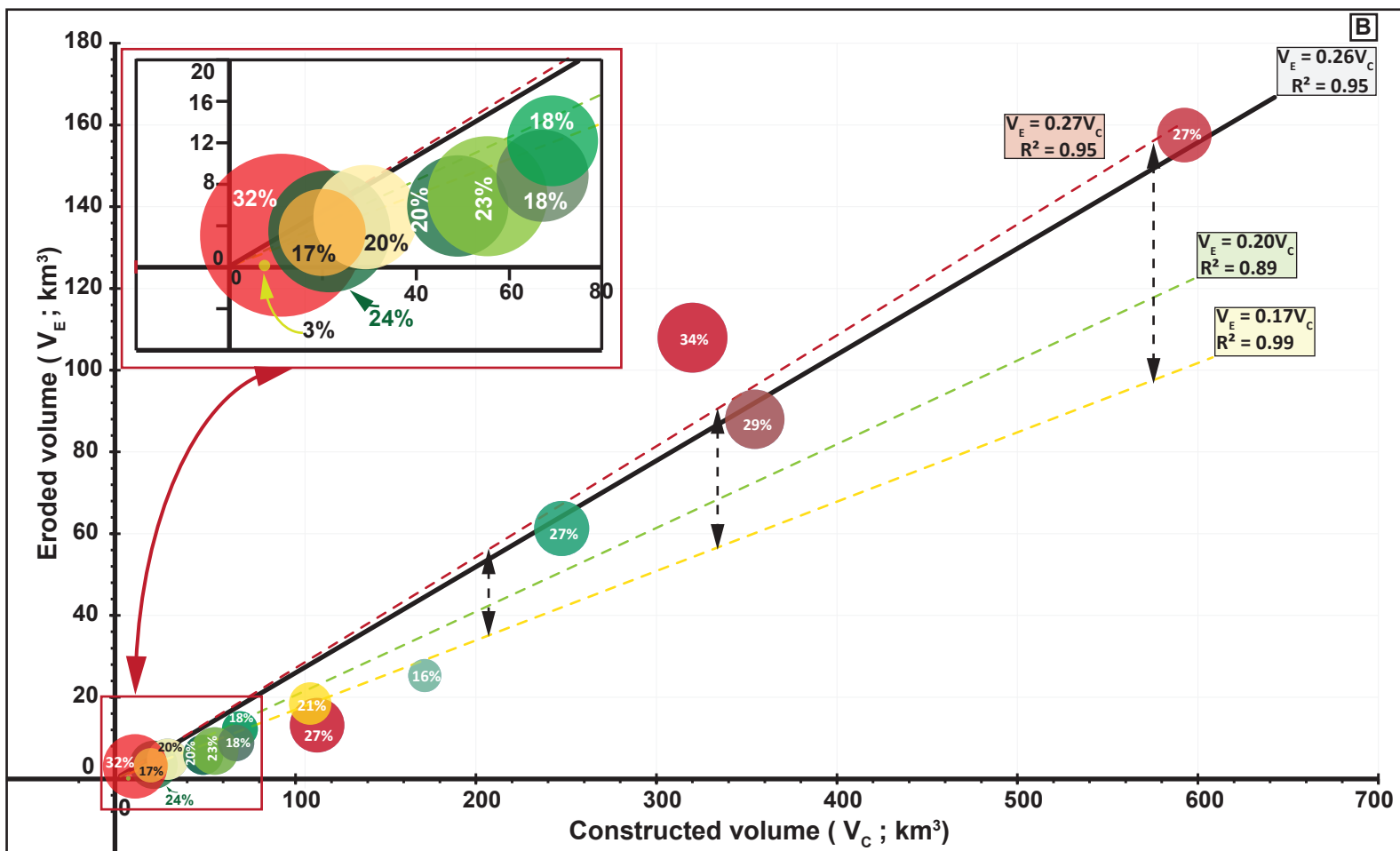
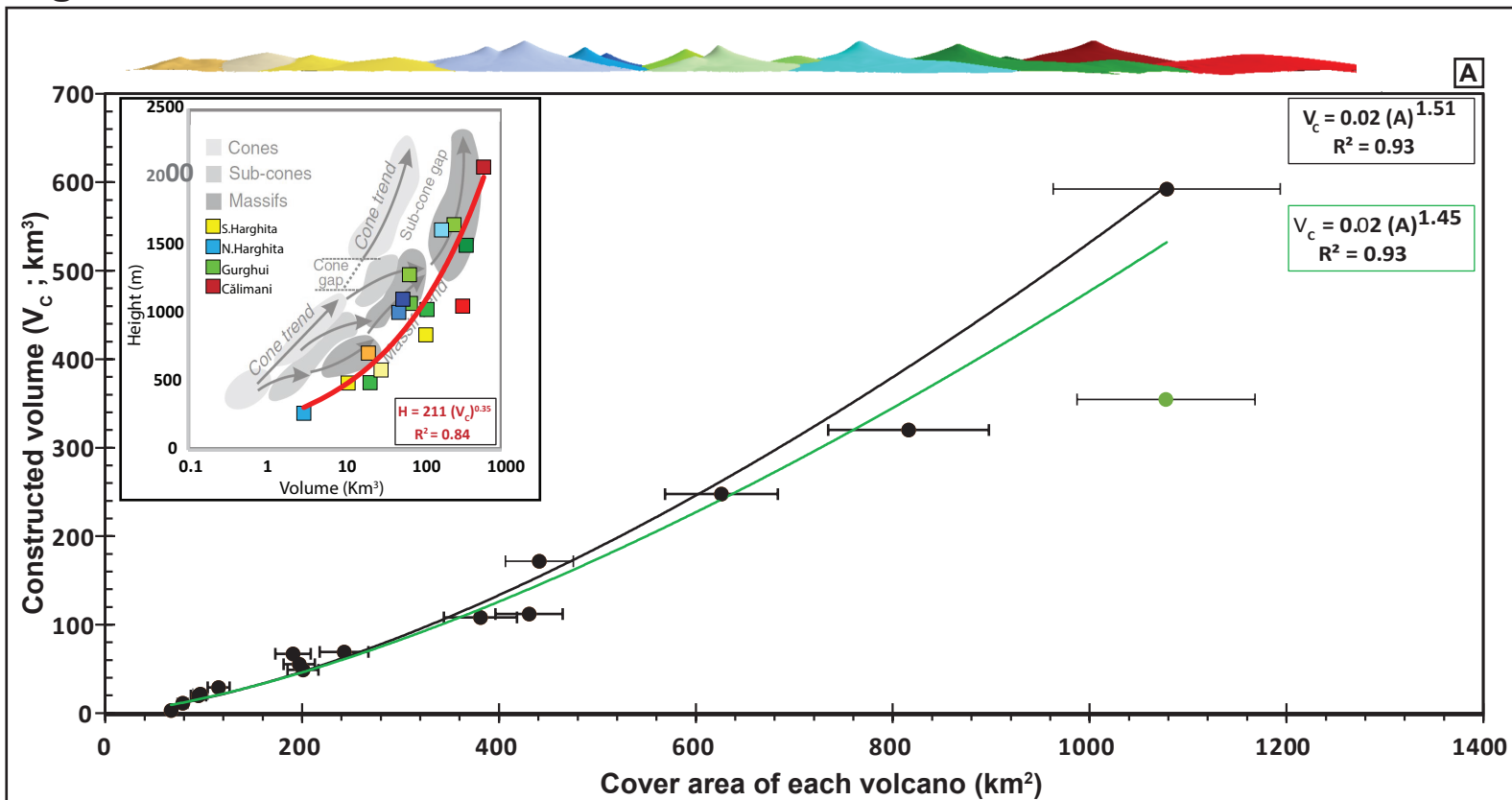


Fig. 6

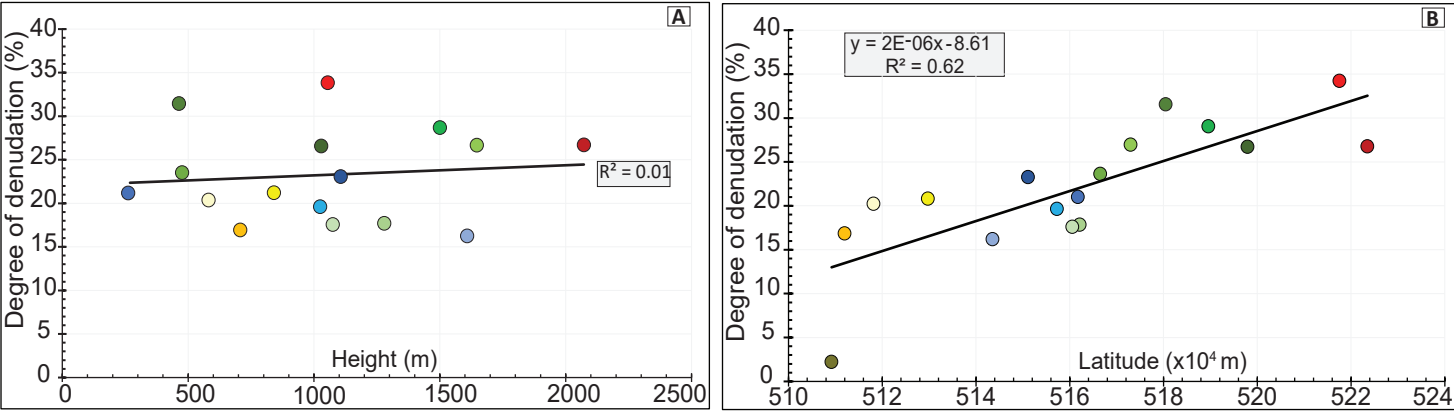


Fig. 7

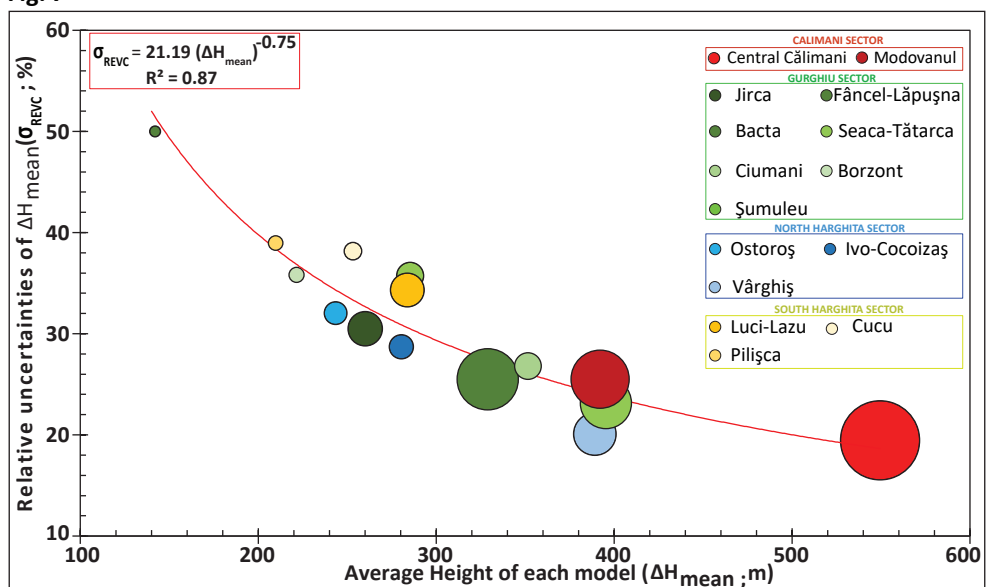


Fig. 8

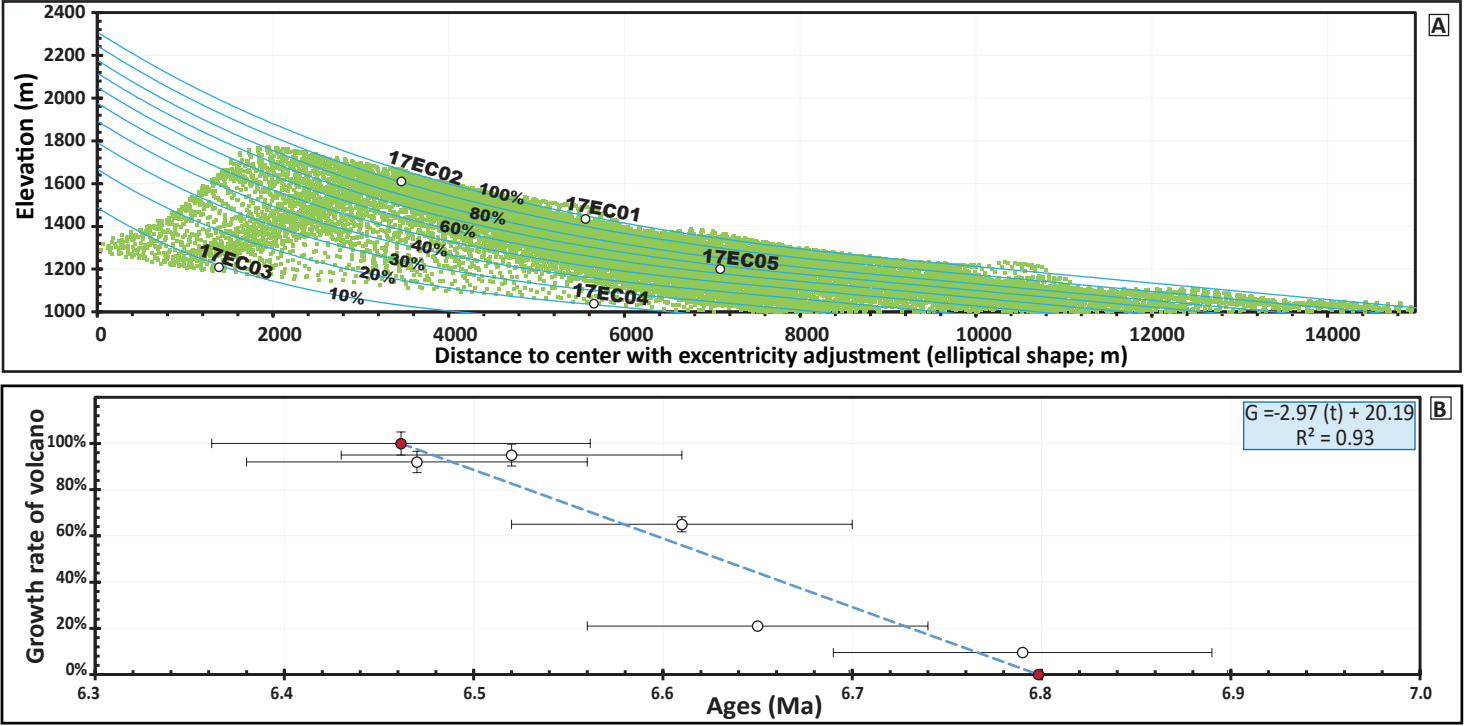


Fig. 9

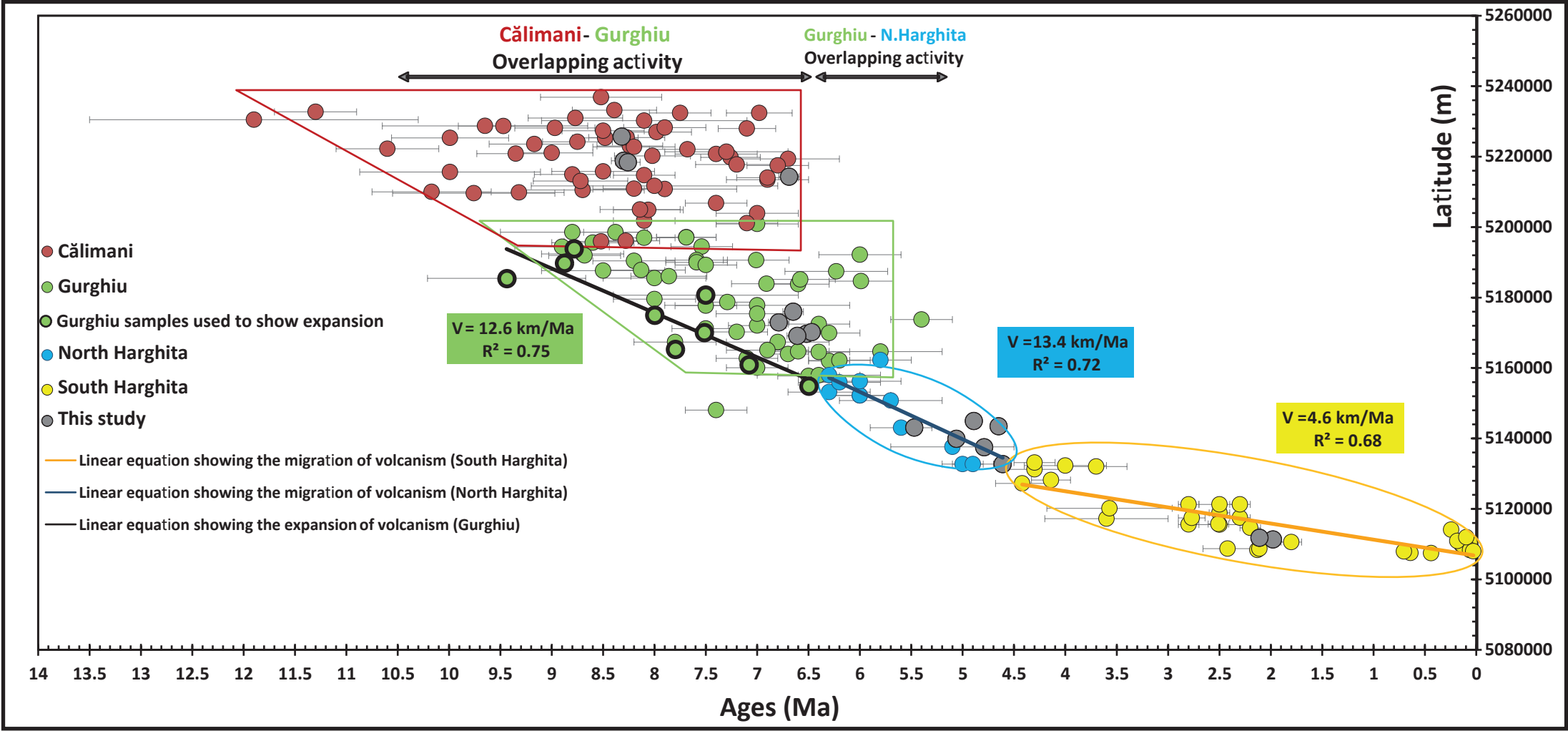


Fig.10

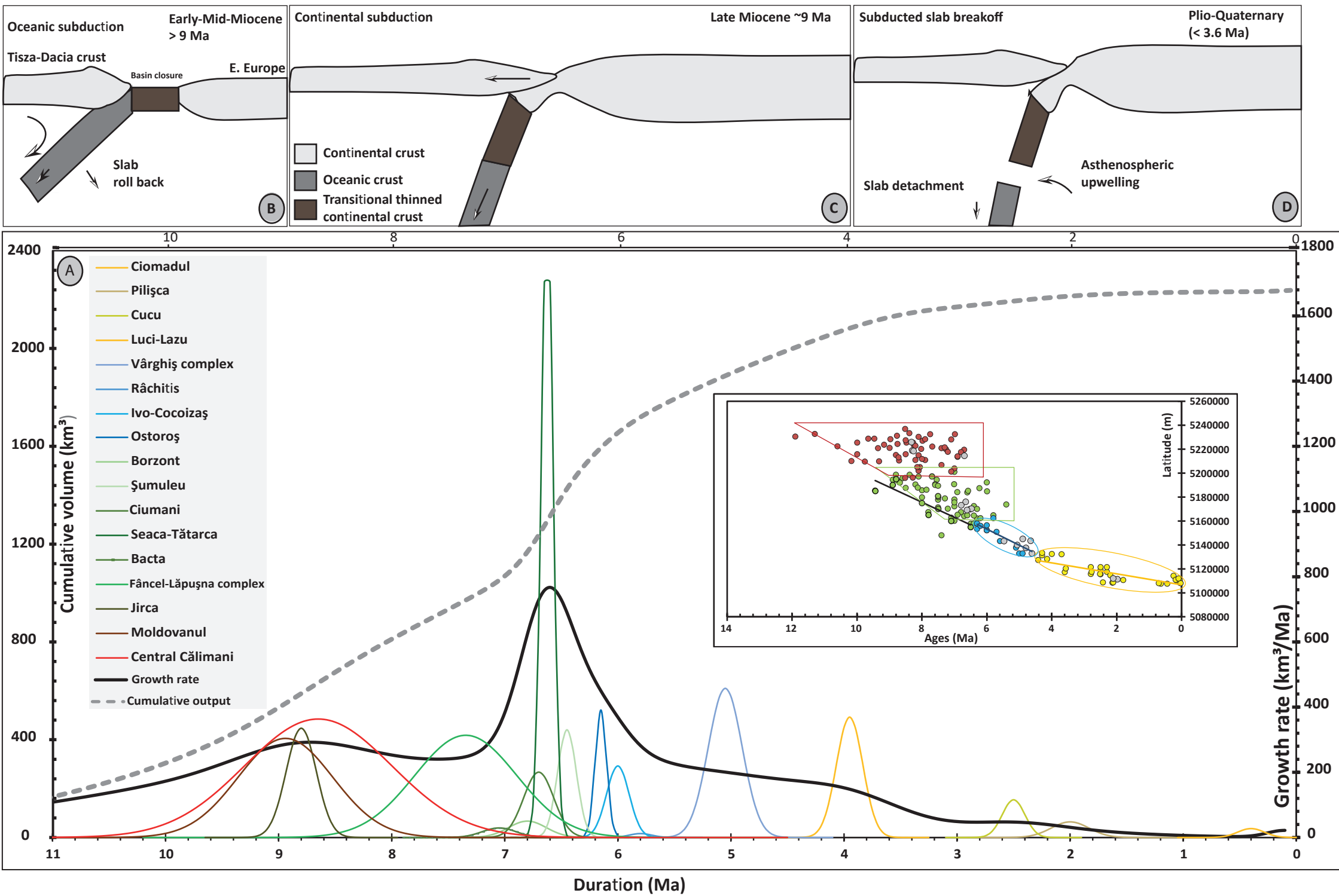


Fig. 11

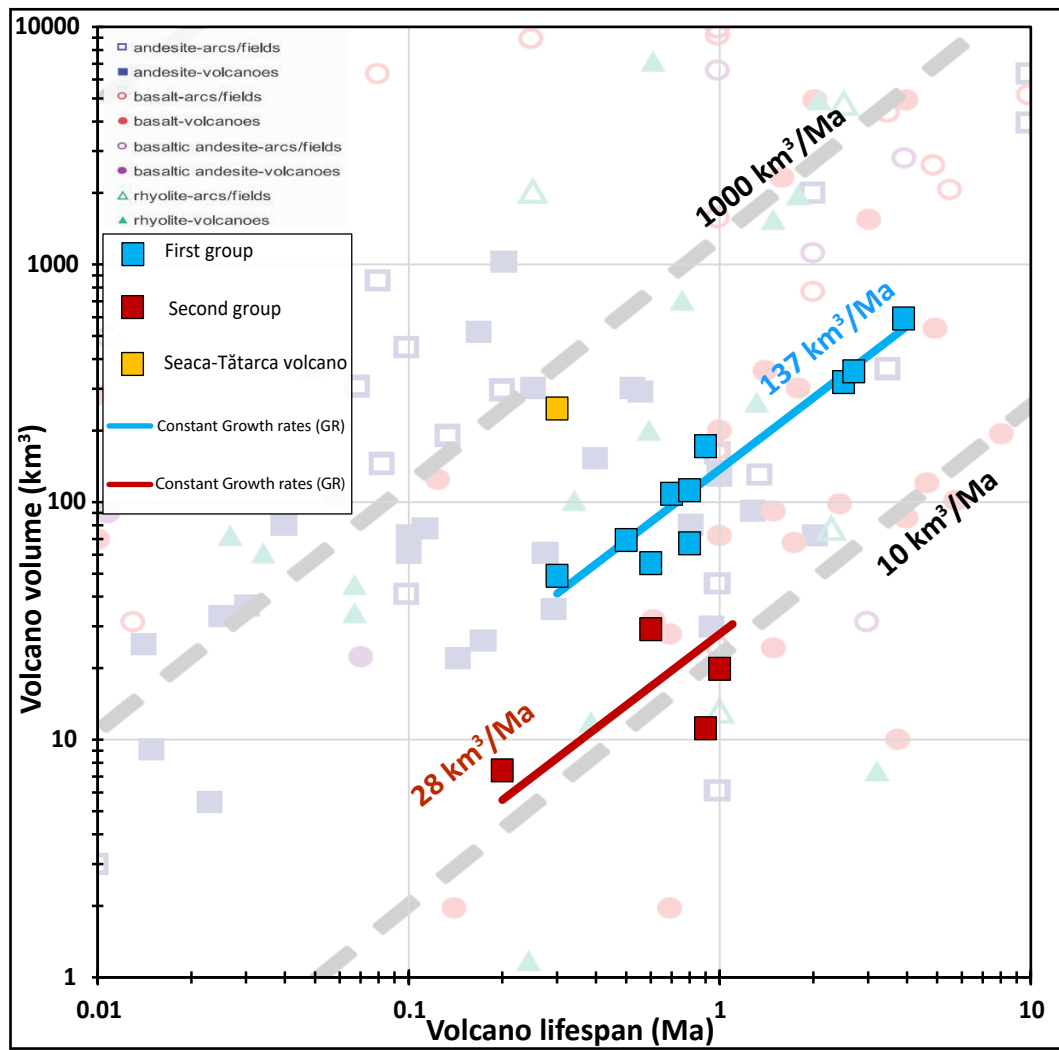
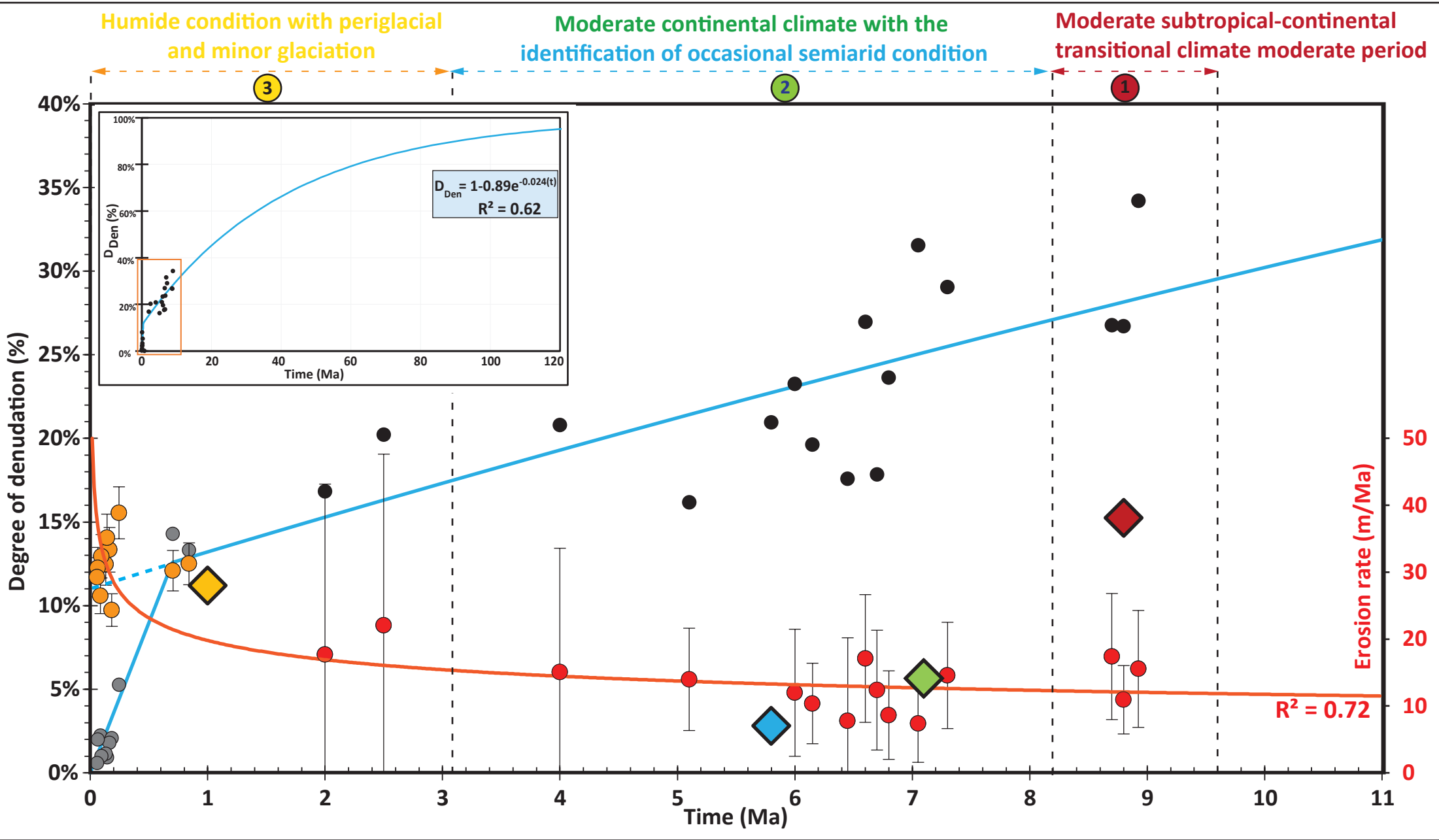


Fig. 12



Tables

Table 1. New K-Ar dating results (details of measurement in S.M).

Sample code	Rock type	K%	Mean age ± 1σ (Ma)	
17EC14	Dacite	2.730	1.98±0.06	Pilișca
17EC15	Dacite	2.841	2.11±0.04	
17EC11	Pyr. andesite	1.503	4.61±0.07	Vârghis
17EC09	Pyr. andesite	1.551	4.65±0.07	
17EC06	Pyr. andesite	1.932	4.79±0.07	
17EC10	Pyr. andesite	1.995	4.89±0.07	
17EC07	Pyr. andesite	1.326	5.06±0.07	
17EC08	Am. andesite	2.373	5.47±0.08	
17EC02	Pyr. andesite	1.219	6.47±0.09	Seaca-Tătarca
17EC01	Pyr. andesite	1.328	6.52±0.09	
17EC05	Pyr. andesite	1.517	6.61±0.09	
17EC04	Pyr. andesite	1.461	6.65±0.09	
17EC03	Pyr. andesite	1.193	6.79±0.10	
17KEL6	Px-Amph And.	1.680	8.33±0.12	Călimani
17P-KEL6	Px-Amph And.	1.648	8.30±0.12	
17KEL5	Monzodiorite	2.755	8.26±0.12	
17KEL1	Dacite	2.291	6.69±0.10	

Table 2. Volumetric data (computed from modelled volcanic uppermost surface) and growth rate for each of CGH volcano (labelled as in Fig. 1) and each CGH sectors (at bottom of the table). Values are quoted with uncertainties at 1σ -level. Constructed volume (V_c , in km^3), degree of denudation (D_{Den}): proportion of volcano lost by dismantling processes (in %). All morphometric values from this study except for Ciomadul volcano (Karátson et al., 2019)

Sector	Label and Volcanoes	Radiometric data			Volumetric data						
		Age _{Beginning} (Ma)	Age _{Ending} (Ma)	Lifespan (ΔT) (Ma)	Visible Area (km^2)	Height (m) a.base.l \pm uncertainty (σ_{ZSV}) (m)	Constructed volume (V_c in km^3)	Growth rate (GR) (km^3/Ma)	Eroded Volume (V_E in km^3)	Erosion rate (ER) (m /Ma)	Degree of Denudation (D_{Den})
Călimani	01 : Central Călimani (Kelemen)	10.6	6.7	3.9	1041	2072 \pm 82	592 \pm 115	152	158 \pm 85	17 \pm 9	27%
	02 : Moldoveanul (Moldováanka)	10.2	7.7	2.5	779	1053 \pm 78	320 \pm 82	128	108 \pm 61	16 \pm 9	34%
Gurghiu	03 : Jirca (Nagy-Erdős)	9.2	8.4	0.8	137	1028 \pm 45	112 \pm 34	140	13 \pm 6	11 \pm 5	27%
	04 : Fâncel-Lăpușna (Fancsal)	8.7	6.0	2.7	828	1499 \pm 58	355 \pm 90	131	88 \pm 48	15 \pm 8	29%
	05 : Bacta (Bakta)	7.5	6.6	0.9	59	490 \pm 41	11 \pm 6	12	3 \pm 2	7 \pm 6	32%
	06 : Seaca-Tătarca (Mezőhavas)	6.8	6.5	0.3	543	1650 \pm 63	248 \pm 57	825	61 \pm 34	17 \pm 10	27%
	07 : Ciumani (Csomafalvi Délhegy)	7.1	6.3	0.8	106	1284 \pm 60	67 \pm 18	84	9 \pm 6	12 \pm 9	18%
	08 : Borzont	-	-	-	59	493 \pm 45	21 \pm 8	-	3 \pm 3	-	24%
	09 : Șumuleu (Somlyó)	6.7	6.2	0.5	242	1073 \pm 80	69 \pm 25	138	12 \pm 19	8 \pm 12	18%
North Harghita	10 : Ostoros (Osztoróc)	6.3	6	0.3	93	1008 \pm 37	49 \pm 16	163	6 \pm 3	10 \pm 6	20%
	11 : Ivo-Cocoizaș (Fertő-tető)	6.3	5.7	0.6	95	1104 \pm 57	55 \pm 16	92	7 \pm 5	12 \pm 10	23%
	12 : Râchitis (Csíkmagosa)	-	-	-	67	269 \pm 24	3 \pm 3	-	1 \pm 2	-	21%
	13 : Vârghiș (Madarasi-Hargita)	5.5	4.6	0.9	355	1611 \pm 39	172 \pm 34	191	25 \pm 14	14 \pm 8	16%
South Harghita	14 : Luci-Lazu (Nagykőbük- Tetőfenyő)	4.3	3.6	0.7	306	843 \pm 74	108 \pm 37	155	18 \pm 23	15 \pm 19	21%
	15 : Cucu (Kakukkhegy)	2.8	2.2	0.6	88	586 \pm 64	29 \pm 11	49	5 \pm 6	22 \pm 26	20%
	16 : Pilișca (Piliske)	2.5	1.5	1.0	95	709 \pm 51	20 \pm 8	20	3 \pm 5	18 \pm 26	17%
	17 : Central Ciomadul (Csomád)	0.2	0.03	0.2	72	-	7 \pm 1	37	0.2 \pm 0.1	26 \pm 4	3%
CGH sector		Activity duration (Ma)		Total volume constructed per area (km^3)		Growth rates per area (km^3/Ma)		Degree of Denudation per sector (D_{Den} %)		Eroded volume (km^3)	Erosion rates (m/Ma)
Călimani		3.9		910 \pm 140		235		30		265 \pm 105	17
Gurghiu		3.4		883 \pm 117		270		25		190 \pm 63	11
North Harghita		2.4		279 \pm 41		116		20		39 \pm 15	9
South Harghita		4.3		165 \pm 40		39		15		27 \pm 24	28
CGH total		~11 Ma		2239\pm192		~200		~ 22		524\pm125	~20

Table 3. Specific erosion rates along CGH range history for each contemporaneous climate period (details in Fig. 12 legend).

Sector	Period of activity (Ma)	Average age (Ma)	Erosion rate (m/Ma)	Climate fluctuation
Călimani	10.8 - 6.9	8.8	38	Short-time moderate period subtropical-continental transitional climate (More Humid; 3)
Gurghiu	8.7 - 5.5	7.1	14	Moderate continental climate (Less humid ; 2)
North Harghita and Luci-Lazu edifice	7- 4.6	5.8	7	Moderate continental climate with the identification of occasional semiarid condition (2)
South Harghita (Cucu, Pilișca, Ciomadul)	<3 - present	1.0	28	Moderate continental Humid condition with periglacial and minor glaciation (1)